PSU-IRL-SCI-410

Classification Numbers 1.5.1

THE PENNSYLVANIA STATE UNIVERSITY

IONOSPHERIC RESEARCH

Scientific Report 410

RELATIONS AMONG LOW IONOSPHERE PARAMETERS AND HIGH FREQUENCY RADIO WAVE ABSORPTION

by

John P. Cipriano

January 9, 1973

The research reported in this document was supported by the U.S. Army Research Office — Durham under contract DA-ARO-D-31-124-72-G158 and by the National Aeronautics and Space Administration under contract NGR-39-009-218.

IONOSPHERE RESEARCH LABORATORY

University Park, Pennsylvania

PSU-IRL-SCI-410
Classification Numbers 1.5.1

Scientific Report 410

Relations Among Low Ionosphere Parameters and High Frequency Radio Wave Absorption

by

John P. Cipriano

January 9, 1973

The research reported in this document was supported by the U. S. Army Research Office - Durham under contract DA-ARO-D-31-124-72-G158 and by the National Aeronautics and Space Administration under contract NGR-39-009-218.

Submitted by: Leslie C. Hale

Leslie C. Hale, Professor of
Electrical Engineering
Project Supervisor

Approved by: Anthony J. Ferraro

Anthony J. Ferraro, Acting Director
Ionosphere Research Laboratory

Ionosphere Research Laboratory

The Pennsylvania State University

University Park, Pennsylvania 16802

ACKNOWLEDGMENTS

The author wishes to express his appreciation to Dr. H. A. Panofsky and Dr. L. C. Hale for their guidance in this research.

The author also wishes to thank Mr. R. O. Olsen and Mrs. B. J. Houston for respectively providing and reducing much of the data required for this work.

TABLE OF CONTENTS

LIST OF TABLES

LIST OF FIGURES

CHAPTER I

INTRODUCTION

1.1 Importance of the Problem

The ionosphere is very complex between 50 and 90 kilometers (Km), where ionization is produced by only the most deeply penetrating radiations. This region is characterized by weakly-ionized plasma and large neutral species density as well as a complex ion chemistry and electron attachment and detachment processes (Whitten and Poppoff, 1971).

Routine measurements of meteorological and ionospheric parameters within this region are restricted by its unique composition and altitude. Meteorological data are quite plentiful below 65 Km, however, they are rare above that level. In contrast, the various radio techniques employed to measure ionospheric parameters are ineffective below about 65 Km. Because meteorological and ionospheric data seldom overlap, the research emphasis has been focused primarily on investigating the several observations of meteorological (stratospheric)-ionospheric coupling.

However, there is also considerable interest in studying other relationships among meteorological and ionospheric parameters throughout the 50-90 Km range. If such relationships exist, they would make possible an understanding of the characteristics of these parameters even when direct measurements are not available. This is

especially true in the case of ionospheric parameters below 60 Km, where ionization production is due to galactic cosmic rays, and therefore an essentially constant ionization production rate can be assumed.

1.2 Previous Related Research

A review of some early observations of meteorological-ionospheric coupling has been given by Bauer (1958). More recently, research has centered on explaining the anomalously high radio wave absorption observed during some winters. This phenomenon is often referred to as the "winter anomaly" in radio wave absorption.

Several authors (Gregory, 1965; Shapley and Beynon, 1965; Belrose, 1967; Rowe, Ferraro, Lee and Mitra, 1969; Sechrist, Mechtly, Shirke and Theon, 1969) have observed that the winter anomaly occurs simultaneously with major stratospheric warmings. A general discussion of the stratospheric warming phenomenon, including coupling with the ionosphere, can be found in Winds and Turbulence in the Stratosphere, Mesosphere, and Ionosphere, edited by Rawer (1968). One explanation for these relationships is in terms of hydrostatic coupling between low-level temperature and high-level density. However, Entsian, Gaygerov and Tarasenko (1971) found no direct, unique relation between hydrostatic coupling and the winter anomaly. Also, Heard (1967) noted a poor correlation between electron density measured at 70 Km and 10 millibar temperature.

Other explanations are based on changes in atmospheric composition, such as variations in ozone and nitric oxide concentrations (Mawdsley, 1961; Belrose, 1967; Sechrist, 1967). The latest evidence suggests that the winter anomaly is due to a variability in the electron loss rate (Geller and Sechrist, 1971; Cipriano, Hale and Mitchell, 1972).

Mitchell and Hale (1972) have qualitatively noted several of the relationships which are analyzed herein.

1.3 Specific Statement of the Problem

In this work, sufficient electrical conductivity data, obtained between 30 and 75 Km by the parachute-borne blunt probe technique (Hale, Hoult and Baker, 1968), are presented so that quantitative relationships among the various meteorological and ionospheric parameters can be determined.

The specific purposes of this work are:

a) To investigate relationships between meteorological and ionospheric parameters which are independent of altitude

b) To determine if electrical parameters measured below 60 Km are coupled with radio wave absorption occurring above that level.

CHAPTER II

DATA REDUCTION

2.1 Electrical Conductivity Data

2.1.1 The Blunt Probe Technique

Positive ($\sigma+$) and negative ($\sigma-$) conductivities are measured subsonically in the very low ionosphere by rocket-launched parachute-borne blunt probe payloads. The probe is similar in operational characteristics to a meteorological rocketsonde such as the Arcasonde, except that a flat plate charged particle sensor and electrometer replace the thermistor.

The procedure followed is to vary the potential (V_p) of the flat plate which consists of a central collecting surface and concentric guard ring of radii a and R respectively. The electric field (E) generated is given by

$$E = \frac{2V_p}{\pi R} \tag{1}$$

and the current ($I_{p\pm}$) to the collecting surface is

$$I_{p\pm} = \frac{2a^2 V_p \sigma_{\pm}}{R} \tag{2}$$

where $\sigma_{\pm}$ are the conductivities of the atmosphere (Hoult, 1965). To remove drift errors in the instrumentation, conductivities are determined from $dI_{p\pm}/dV_p$ rather than $I_{p\pm}/V_p$, where V_p is established by applying a linear sweep

voltage (V_s) between the probe and return electrode. For V_p greater than several volts

$$\frac{dI_{p\pm}}{dV_p} \simeq \frac{dI_{p\pm}}{dV_s} \tag{3}$$

and therefore (2) becomes

$$\sigma_{\pm} \simeq \frac{R}{2a^2} \frac{dI_{p\pm}}{dV_s} \tag{4}$$

Both pre-launch calibration and in-flight conductivity data are telemetered at 1680 MHz to a GMD type meteorological recording system. This system, with the addition of an external two-track (data and timing channels) tape recorder, acquires the data.

2.1.2 Procedure for Determining Conductivities

Utilizing tape playback equipment, a data "tachometer" and a two-track hot-pen recorder, both calibration and conductivity data are converted from tape to a strip chart recording of current as a function of time (t). Sample calibration and conductivity curves are shown in Figure 1, the latter curve being somewhat typical at about 55 Km. The quantities $dI_{p\pm}/dV_s$ in (4) are computed from the slopes given in Figure 1 by

$$\frac{dI_{p\pm}}{dV_s} = \frac{1}{R_{cal}} \frac{(dI_{p\pm}/dt)}{(dI/dt)_{cal}} \tag{5}$$

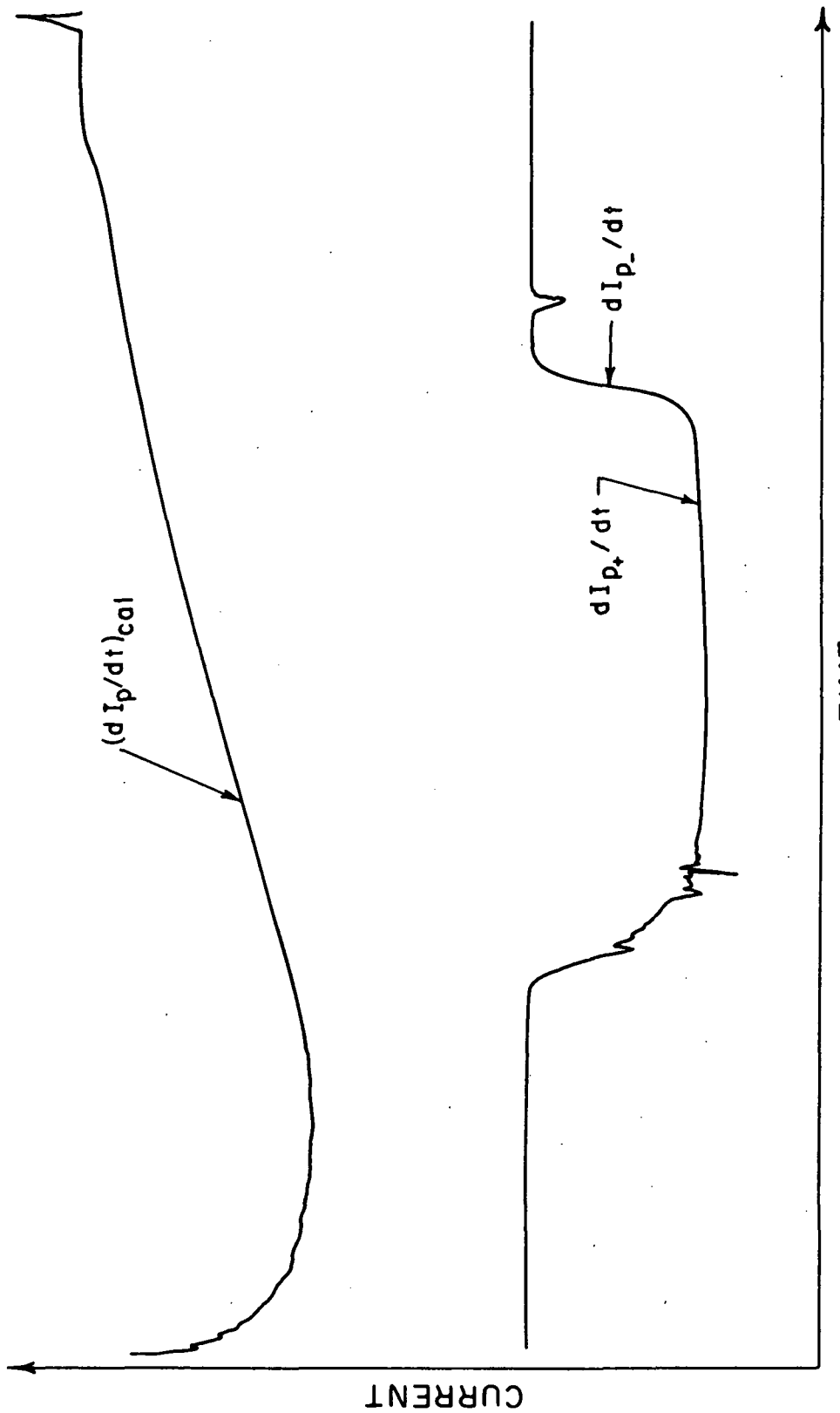

Figure 1. Calibration and Conductivity Curves

where R_{cal} is the calibration resistance. Substituting (5) into (4) yields

$$\sigma_{\pm} \simeq \frac{R}{2a^2 R_{cal}} \frac{(dI_{p\pm}/dt)}{(dI/dt)_{cal}} \qquad (6)$$

which gives $\sigma_{\pm}$ as functions of time.

The probe's position is continuously monitored by ground based radar, allowing the conductivities to be plotted as functions of altitude (z). Response limitations of the system prohibit accurate measurements of dI_{p-}/dt above 63 Km, and therefore σ_- is not computed above this level.

2.1.3 The Conductivity Data

Between January 22, 1971 and February 1, 1972, conductivity data were obtained from 10 blunt probes launched at White Sands Missile Range (WSMR), New Mexico, and NASA Wallops Island (WI), Virginia (see Table 1). Data from six of these launches have been previously reported by Mitchell and Hale (1972). Conductivities obtained on January 19, 1972, are given in Figure 2, while smoothed curves representing conductivity data for each of the launches are presented in Figures 3 and 4, the dashed line being the average curve for all 10 launches.

Figures 3 and 4 indicate that day-to-day variations can be quite large for both positive and negative conductivities. For example, σ_+ values determined on

Table 1

Parameters for Blunt Probe Launchings

Date	Local Time (Hours)	Solar Zenith Angle (Degrees)	Apogee (Km)	Location
22 Jan 71	1300	54	77	WSMR
26 Jan 71	1430	62	79	WSMR
1 Feb 71	1215	50	78	WSMR
9 Jun 71	0810	53	79	WSMR
28 Jul 71	0705	68	78	WSMR
13 Oct 71	1050	44	77	WSMR
6 Jan 72	1337	64	67	WI
19 Jan 72	1230	53	70	WSMR
31 Jan 72	1307	59	82	WI
1 Feb 72	1200	51	73	WSMR

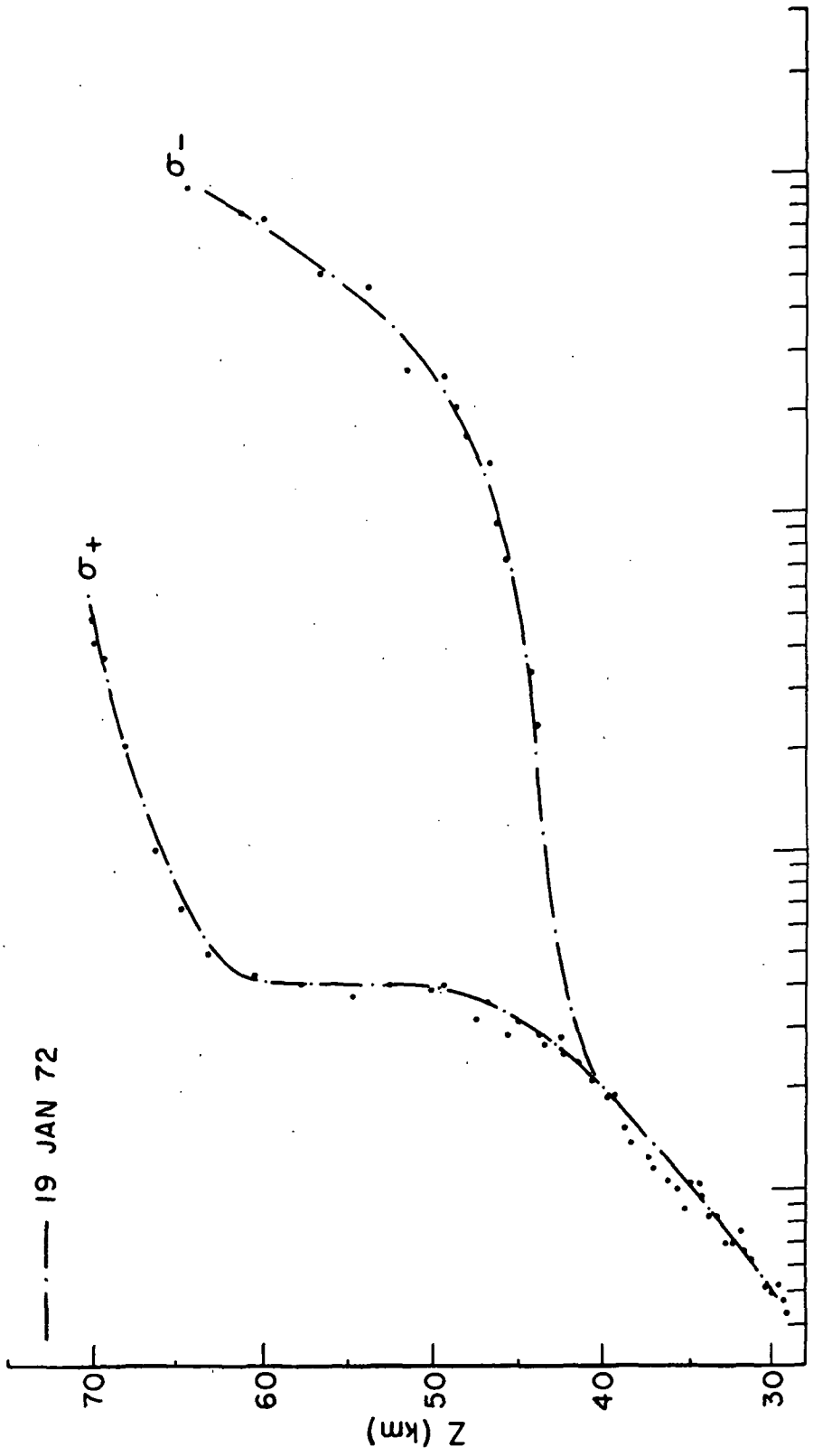

Figure 2. January 19, 1972 Conductivity Data

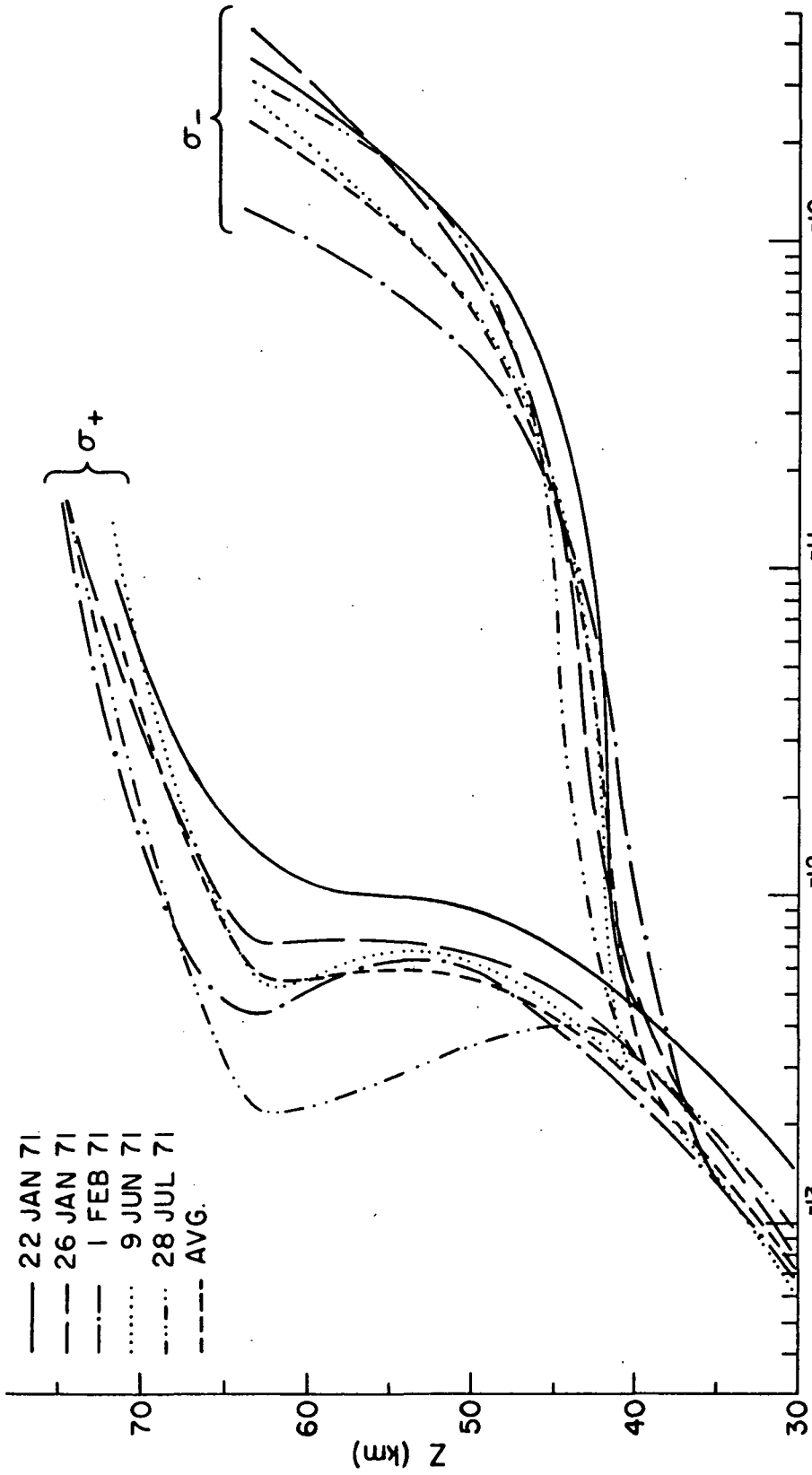

Figure 3. Smoothed Conductivity Curves

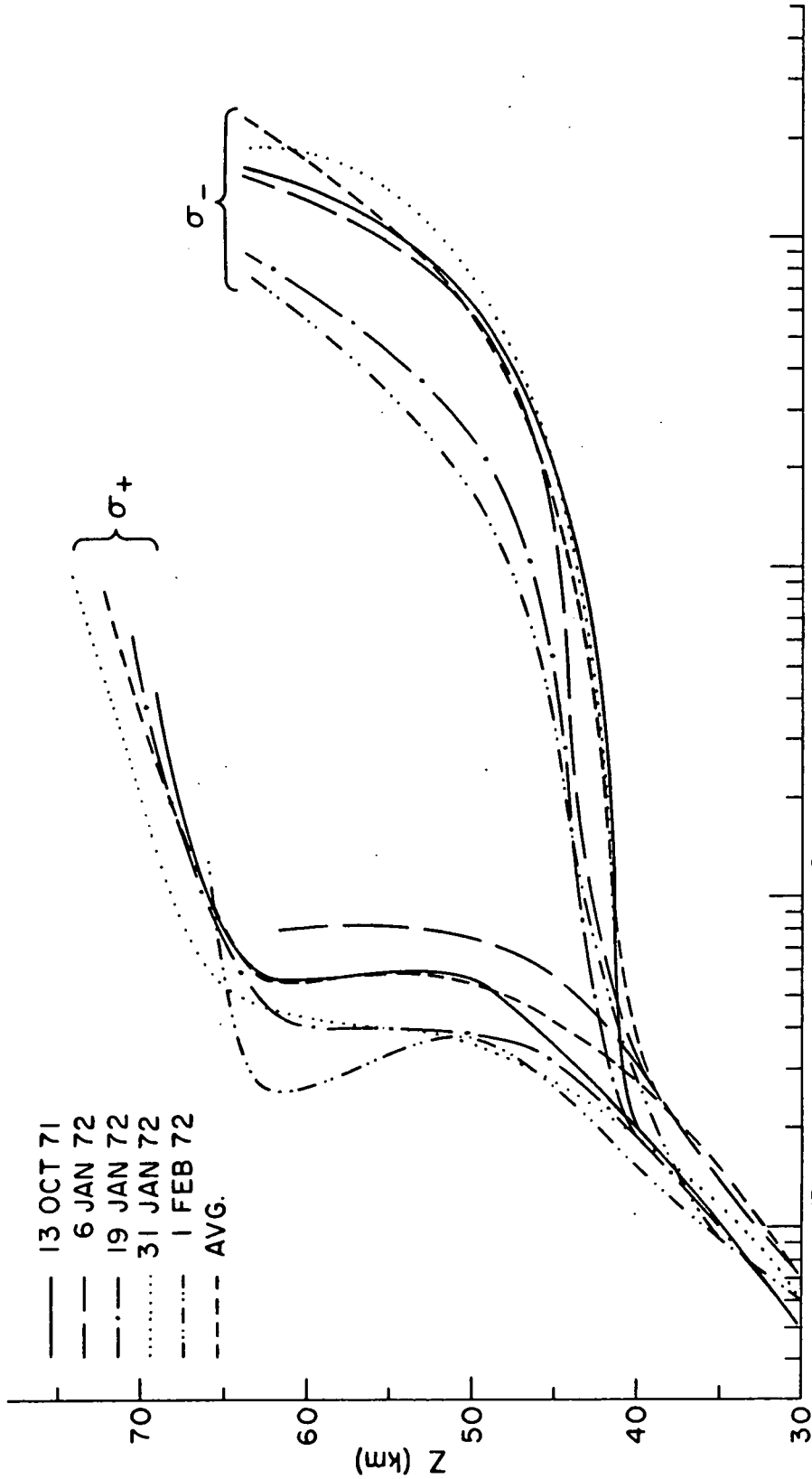

Figure 4. Smoothed Conductivity Curves

January 22, 1971, are up to five times greater than those of July 28, 1971, and σ- values for January 26, 1971, are about a factor of five greater than those of February 1, 1972.

2.2 Meteorological Data

Meteorological data are provided by the Loki Dart system of the Meteorological Rocket Network (MRN) which measures upper atmospheric temperature (T) by means of a bead thermistor sensor (Ballard and Rofe, 1969). Atmospheric density (ρ) and pressure (P) are then calculated from the hydrostatic relation and a reference pressure obtained from supporting radiosonde data (Olsen, 1972).

On three occasions, indirect methods were required to determine meteorological parameters. No MRN data were available on January 26, 1971, and values of T, ρ and P were obtained by averaging data from January 25 (0930 MST) and 27 (1200 MST), 1971. The radiosonde reference pressure was in error on June 9, 1971, and this information was provided by the June 9 (0500 MST), 1971 National Meteorological Center's 10 millibar chart. On January 6, 1972, MRN data were not available above 50 Km, and temperatures for this region were determined by averaging the January 5 (1500 EST) and 7 (1000 EST), 1972 values. Except for the above cases, and July 28, 1971, all meteorological data were measured within three hours of the blunt probe launches (see Table 2).

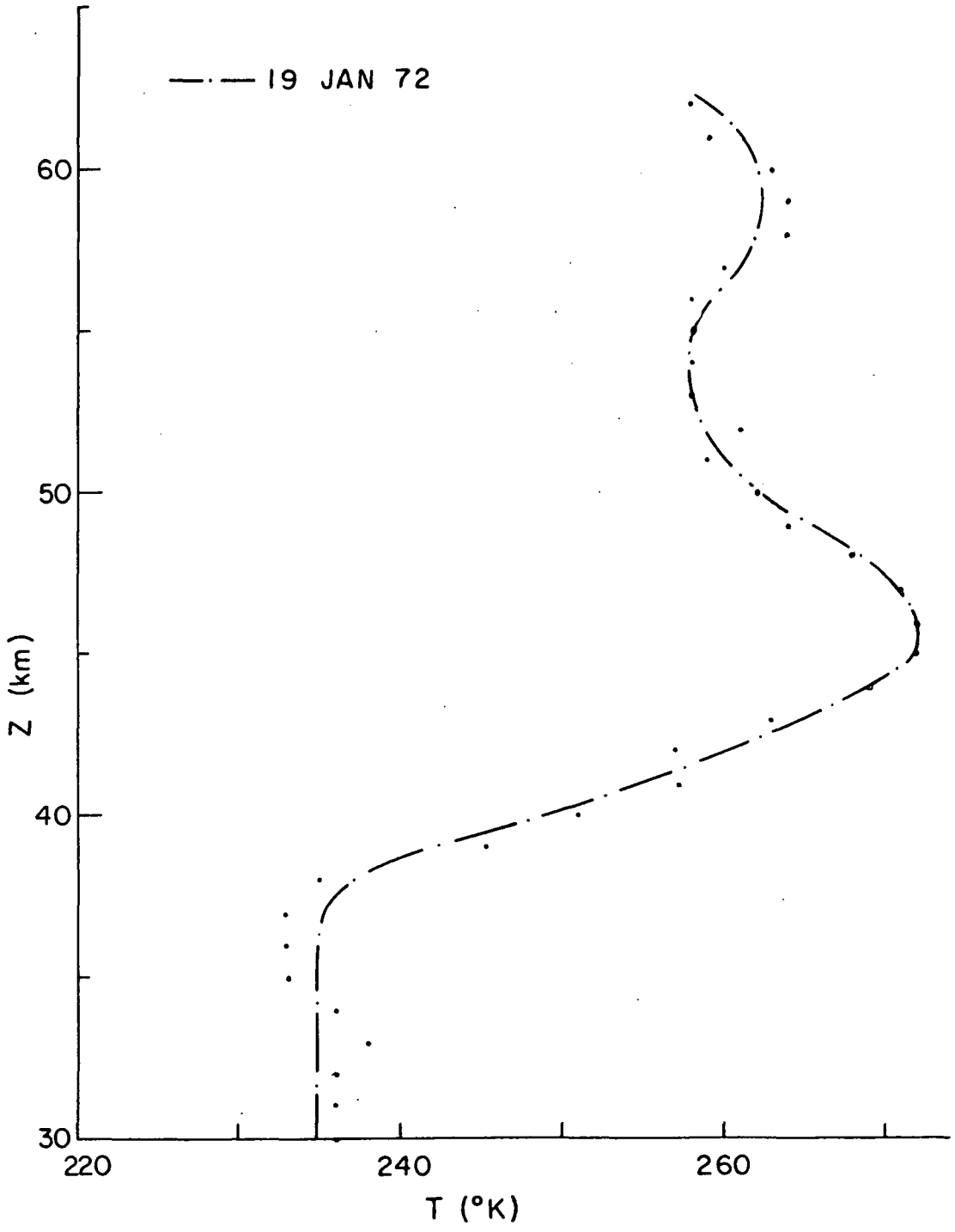

Figure 5. January 19, 1972 Temperature Data

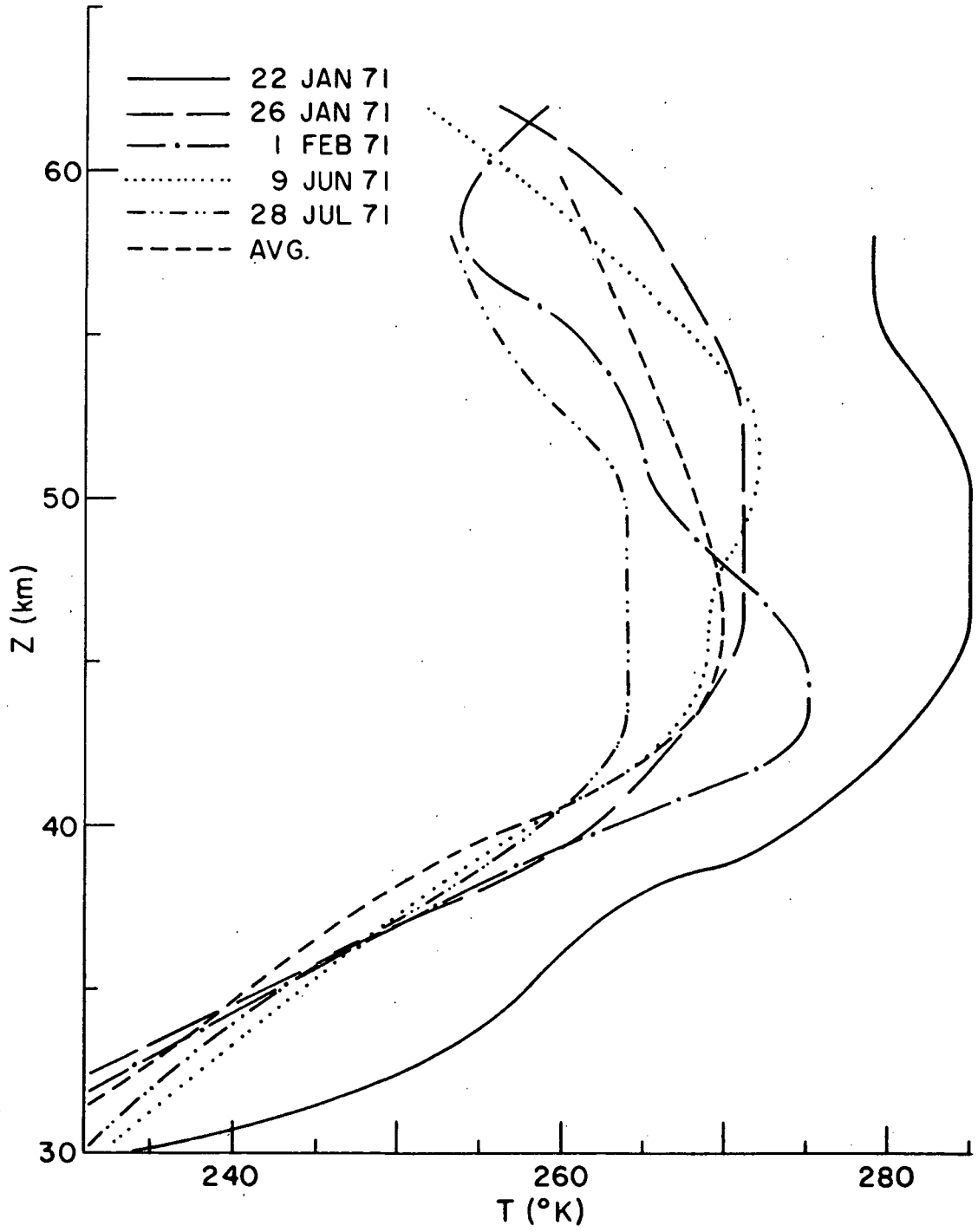

Figure 6. Smoothed Temperature Profiles

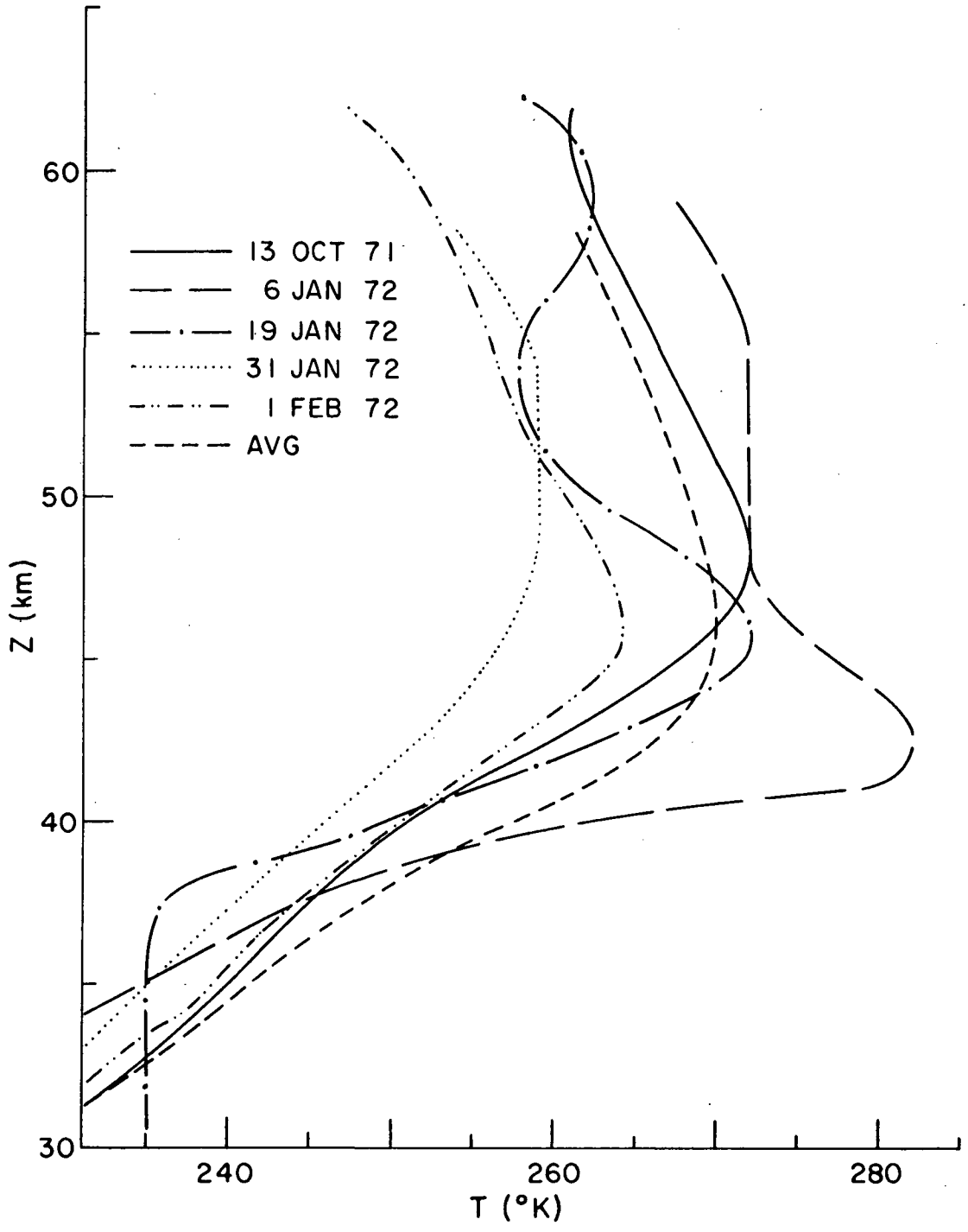

Figure 7. Smoothed Temperature Profiles

Table 2

Loki Dart Launch Times

Date	Local Time (Hours)	Δt* (Hours)	Location
22 Jan 71	1600	3.00	WSMR
26 Jan 71	xx	xx	WSMR
1 Feb 71	1000	-2.25	WSMR
9 Jun 71	0930	1.33	WSMR
28 Jul 71	1130	4.42	WSMR
13 Oct 71	0845	-2.08	WSMR
6 Jan 72	1430	0.88	WI
19 Jan 72	1030	-2.00	WSMR
31 Jan 72	1405	0.97	WI
1 Feb 72	1030	-1.50	WSMR

*Δt = Loki Launch Time - Blunt Probe Launch Time

Temperatures for January 19, 1972, are given in Figure 5, and smoothed temperature profiles are shown in Figures 6 and 7 which indicate that day-to-day variations in temperature are quite small, seldom exceeding 10 per cent.

2.3 High Frequency Radio Wave Absorption

2.3.1 The Absorption Measurements

High frequency (HF) radio wave absorption data were obtained from the A3 continuous wave technique as described in IQSY Instruction Manual No. 4 Ionosphere (ICSU, 1963). Such measurements were made at WSMR by monitoring the 5.00 MHz radio signal from WWV in Fort Collins, Colorado. A 3.36 MHz signal from Annapolis, Maryland to University Park, Pennsylvania provided absorption data concurrent with the WI blunt probe launches, these data being provided by J. N. Rowe, A. J. Ferraro and H. S. Lee of the Ionosphere Research Laboratory, University Park, Pennsylvania.

The A3 method yields results representative of absorption at the mid-point of the transmitter-to-receiver path. Thus it can be seen from Table 3, which contains geographical coordinates of the transmitting, receiving and launching facilities, that both paths provide absorption data representative of locations far removed from the blunt probe launch sites. At WSMR the distance between the launch facility and the transmitter-to-receiver mid-point is about 470 Km, while for the WI experiment this distance

Table 3

Coordinates of the Transmitting, Receiving and Launching Facilities

Location	Type	Longitude (Degrees)	Latitude (Degrees)
University Park	Receiving	-78.0E	40.8N
Annapolis	Transmitting	-76.5E	39.0N
Wallops Island	Launching	-75.4E	37.8N
White Sands Missile Range	Receiving and Launching	-106.5E	32.4N
Fort Collins	Transmitting	-105.1E	40.6N

is about 310 Km. Absorption over both paths takes place almost entirely above 60 Km (Lee, 1973), where ionization production is principally due to solar ultraviolet (UV) radiation.

2.3.2 Relative Absorption

To facilitate day-to-day comparisons, absorption data are determined relative to the mean absorption level of the previous night. This relative absorption (L) is given by

$$L = 20 \log_{10} \frac{A}{A_o} \tag{7}$$

where A is the measured signal field strength and A_o the average signal intensity of the preceding night. Relative absorption data were determined for each blunt probe launch date, and portions of the February 1, 1972 data are shown in Figure 8. Smoothed curves representing relative absorption data as functions of time are presented in Figures 9 and 10, where the WI absorption scale has been shifted to correspond with the WSMR scale on days of low absorption (Rowe and Hale, 1972).

Figures 9 and 10 indicate that day-to-day variations in relative absorption can be very large, especially in the early afternoon. For example, L values observed at that time on January 26, 1971, are about 20 decibels (Db) higher than those recorded just six days later. From (7), this 20 Db difference translates into an order of magnitude

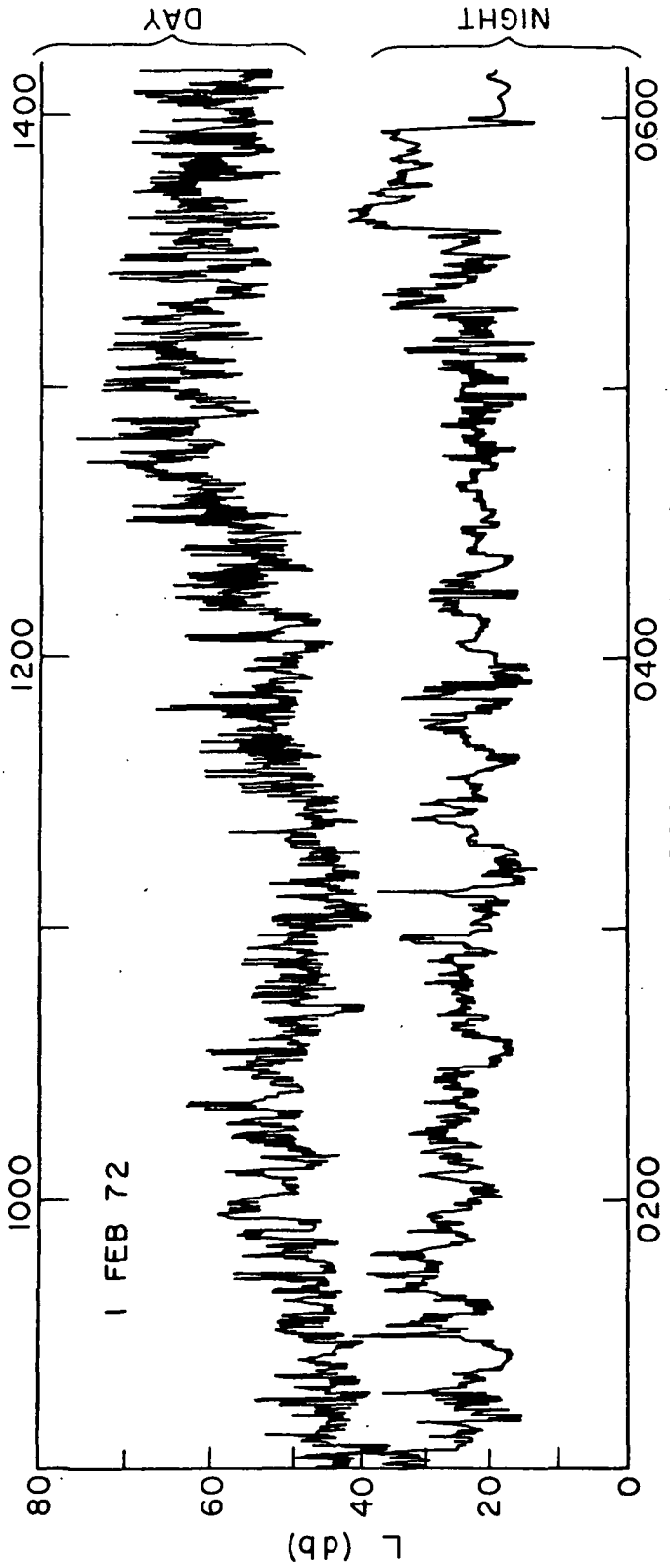

Figure 8. February 1, 1972 Absorption Data

variation in the quantity A/A_o. No evidence of strong solar flare activity was found in any of these data.

The following relative absorption values are analyzed in Sections 4.3.2, 4.3.3 and 4.3.4 respectively:

a) L_n, defined by L at the time the sun's hour angle (Ψ) is 0^o. (This occurs about 1203 and 1209 Local Time at WSMR and WI respectively, and therefore L_n is referred to as the relative noon absorption.)

b) $L_{\chi(\text{AM or PM})}$, defined by L at the times the solar zenith angle (χ) is nearest 60^o. (A zenith angle of 60^o was chosen after Sechrist et al., 1969.)

c) L_p, defined by L at the time of blunt probe launch.

Solar zenith angles are computed from the standard relation

$$\cos \chi = \cos \delta \cos \Psi \cos \phi + \sin \delta \sin \phi \qquad (8)$$

where δ is the solar declination and ϕ the latitude. Table 4 contains the times and zenith angles corresponding to their respective absorptions, where the latitudes and longitudes required for determining χ, Ψ and ϕ are taken from the mid-points of their respective absorption paths.

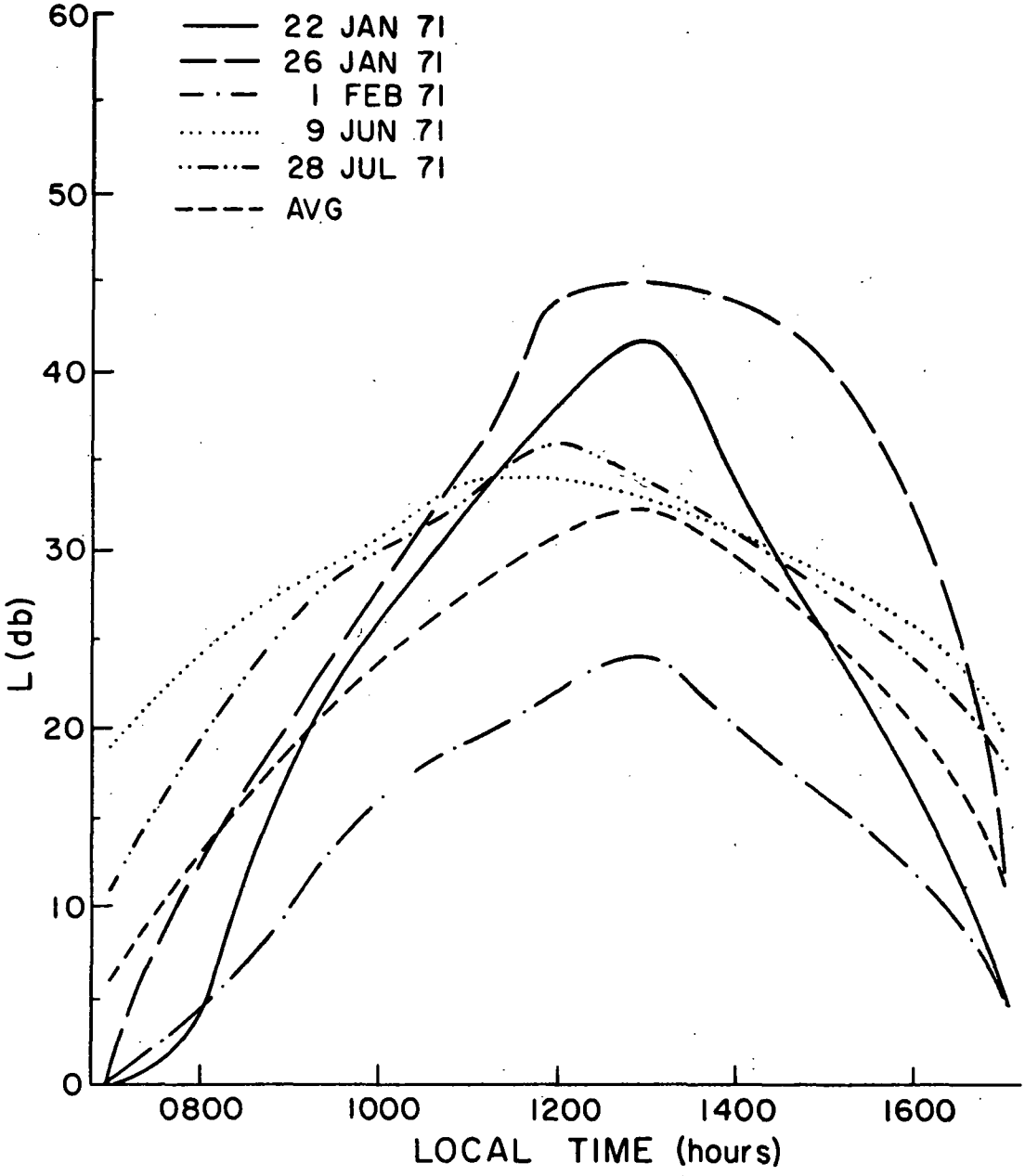

Figure 9. Smoothed Relative Absorption Curves

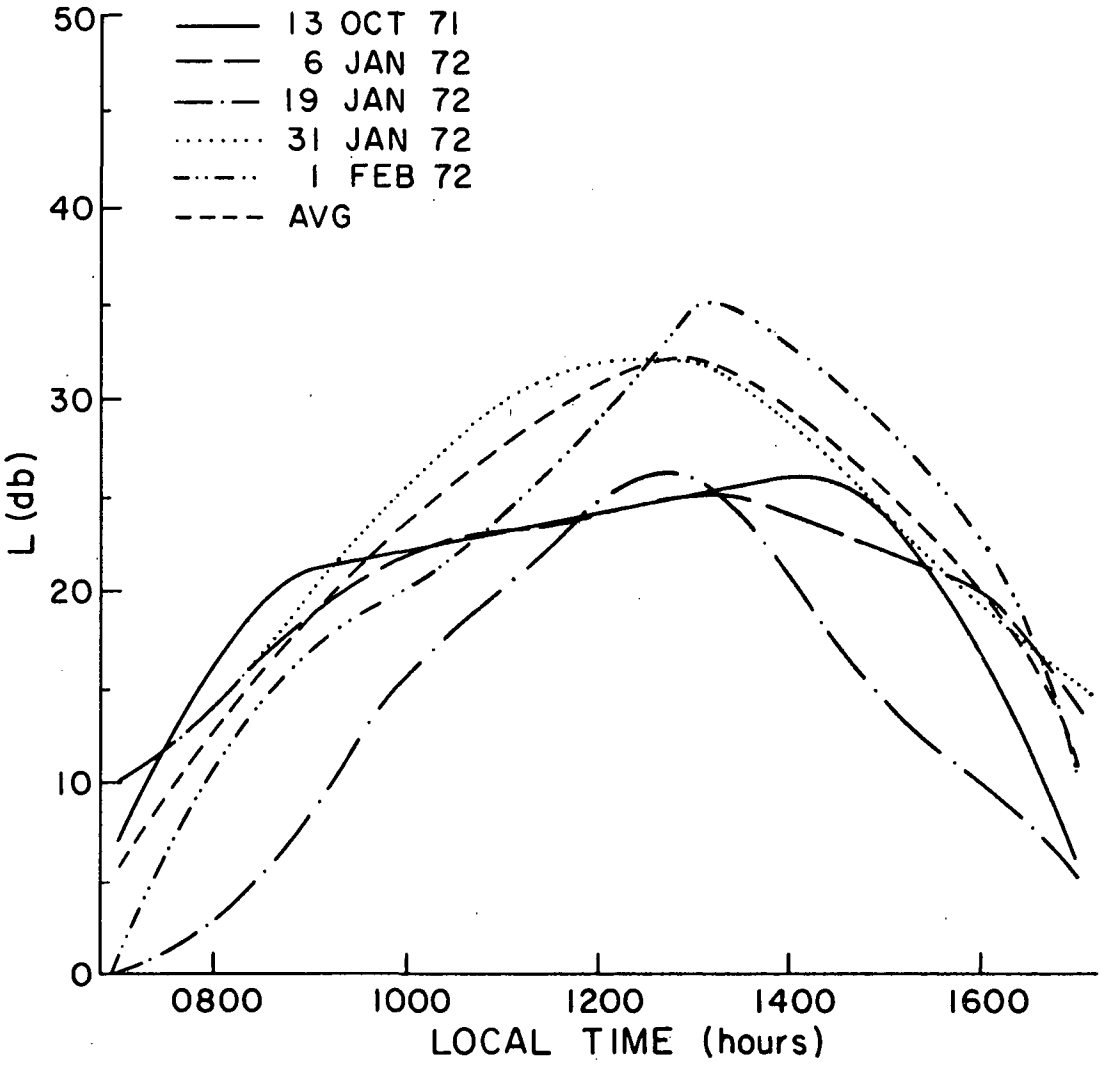

Figure 10. Smoothed Relative Absorption Curves

Table 4

Times and Zenith Angles for their Respective Absorption Values

Date/ Location	Type Absorption	Local Time (Hours)	Solar Zenith Angle (Degrees)
22 Jan 71/ WSMR	L_n	1203	57
	$L_{\chi PM}$	1324	60
	L_p	1300	59
26 Jan 71/ WSMR	L_n	1203	56
	$L_{\chi PM}$	1334	60
	L_p	1430	66
1 Feb 71/ WSMR	L_n	1203	55
	$L_{\chi PM}$	1346	60
	L_p	1215	55
9 Jun 71/ WSMR	L_n	1203	14
	$L_{\chi PM}$	1637	60
	L_p	0810	52
28 Jul 71/ WSMR	L_n	1203	17
	$L_{\chi PM}$	1629	60
	L_p	0705	48
13 Oct 71/ WSMR	L_n	1203	44
	$L_{\chi PM}$	1455	60
	L_p	1050	48
6 Jan 72/ WI	L_n	1209	63
	$L_{\chi PM}$	1200	63
	L_p	1337	66
19 Jan 72/ WSMR	L_n	1203	57
	$L_{\chi PM}$	1316	60
	L_p	1230	58

Table 4 (Cont'd.)

31 Jan 72/ WI	L_n	1209	58
	L_{XPM}	1311	60
	L_p	1307	60
1 Feb 72/ WSMR	L_n	1203	55
	L_{XPM}	1348	60
	L_p	1200	55

CHAPTER III

CHARGED PARTICLE DENSITIES

3.1 Positive Ion Densities

Assuming a small ion model (Hale, 1967), positive ion densities (N+) can be derived from the measured conductivity data by the relation

$$N+ = \frac{\sigma_+}{e\mu+} \tag{9}$$

where e is the electronic charge and $\mu+$ the averaged positive ion mobility.

The mobility of a single ionic species is given by (Dalgarno, 1962; McDaniel, 1964)

$$\mu = \mu_o \frac{T\ P_o}{T_o P} \tag{10}$$

where P_o and T_o are the reference sea level pressure and temperature respectively, and μ_o the reduced mobility, which is assumed to be 1.8 $cm^2V^{-1}sec^{-1}$ for positive ions (Loeb, 1955, Cole and Pierce, 1965). Substituting (10) into (9) yields

$$N+ = \frac{\sigma_+ T_o P}{e\mu_{o+} T\ P_o} \tag{11}$$

Smoothed curves of positive ion densities as functions of altitude are given in Figures 11 and 12, the dashed line

being the average curve for all 10 launches. These data are subject to the uncertainties in the assumed mobility.

Because MRN Loki Darts did not reach the altitudes achieved by the blunt probes, the N+ curves do not extend as high as those for σ_+. However, if T and P values are obtained from the COSPAR International Reference Atmosphere, 1965 (CIRA 65), then N+ values can be estimated wherever σ_+ data are available. The average N+ profile, calculated from CIRA 65 and blunt probe data, is shown in Figure 13. Figures 11, 12 and 13 indicate that positive ion densities experience minimum values between 63 and 66 Km, suggesting the region where ionization production by solar UV radiation supplants production by galactic cosmic rays occurring at the lower altitudes (Mitchell and Hale, 1972).

3.2 Electron Densities

Negative conductivity is given by the sum of negative ion and electron conductivies, that is

$$\sigma_- = N_- e\mu_- + N_e e\mu_e \qquad (12)$$

where N_- and N_e are negative ion and electron densities respectively, and μ_- and μ_e are their respective mobilities. Conservation of charge requires that

$$N_- = N_+ - N_e \qquad (13)$$

and substituting (13) into (12) gives

$$\sigma_- = (N_+ - N_e) e\mu_- + N_e e\mu_e \qquad (14)$$

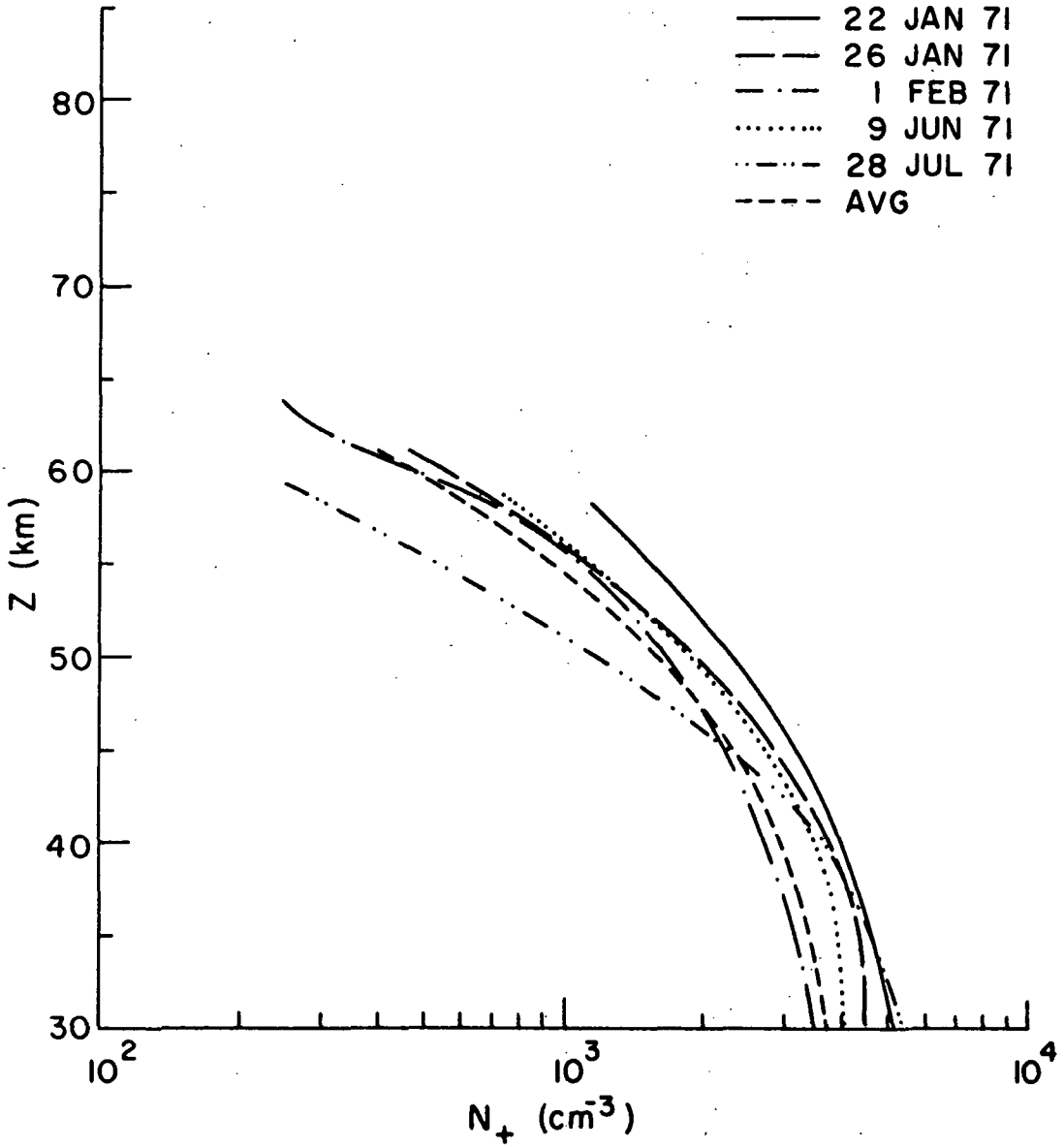

Figure 11. Smoothed Positive Ion Density Profiles

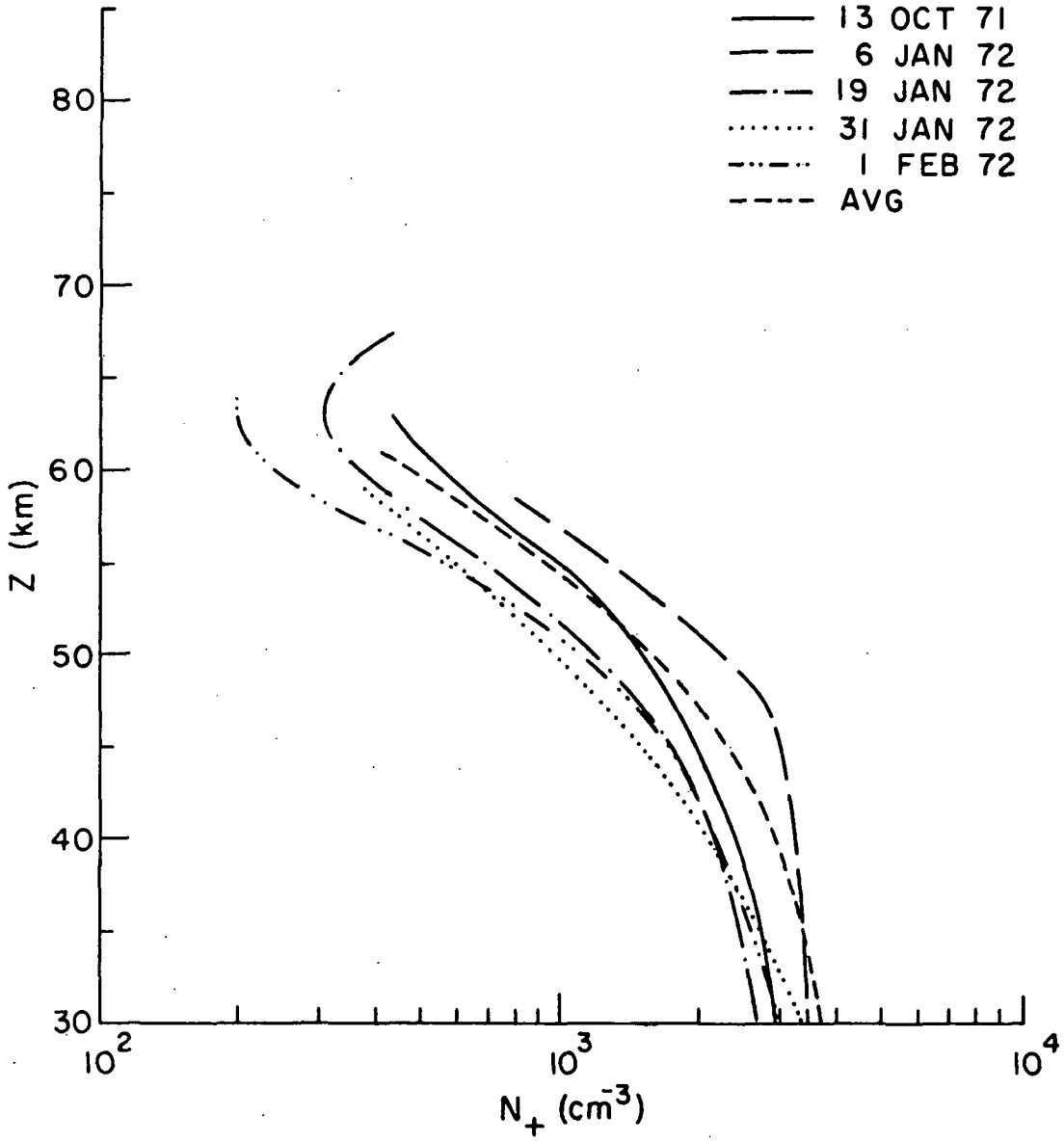

Figure 12. Smoothed Positive Ion Density Profiles

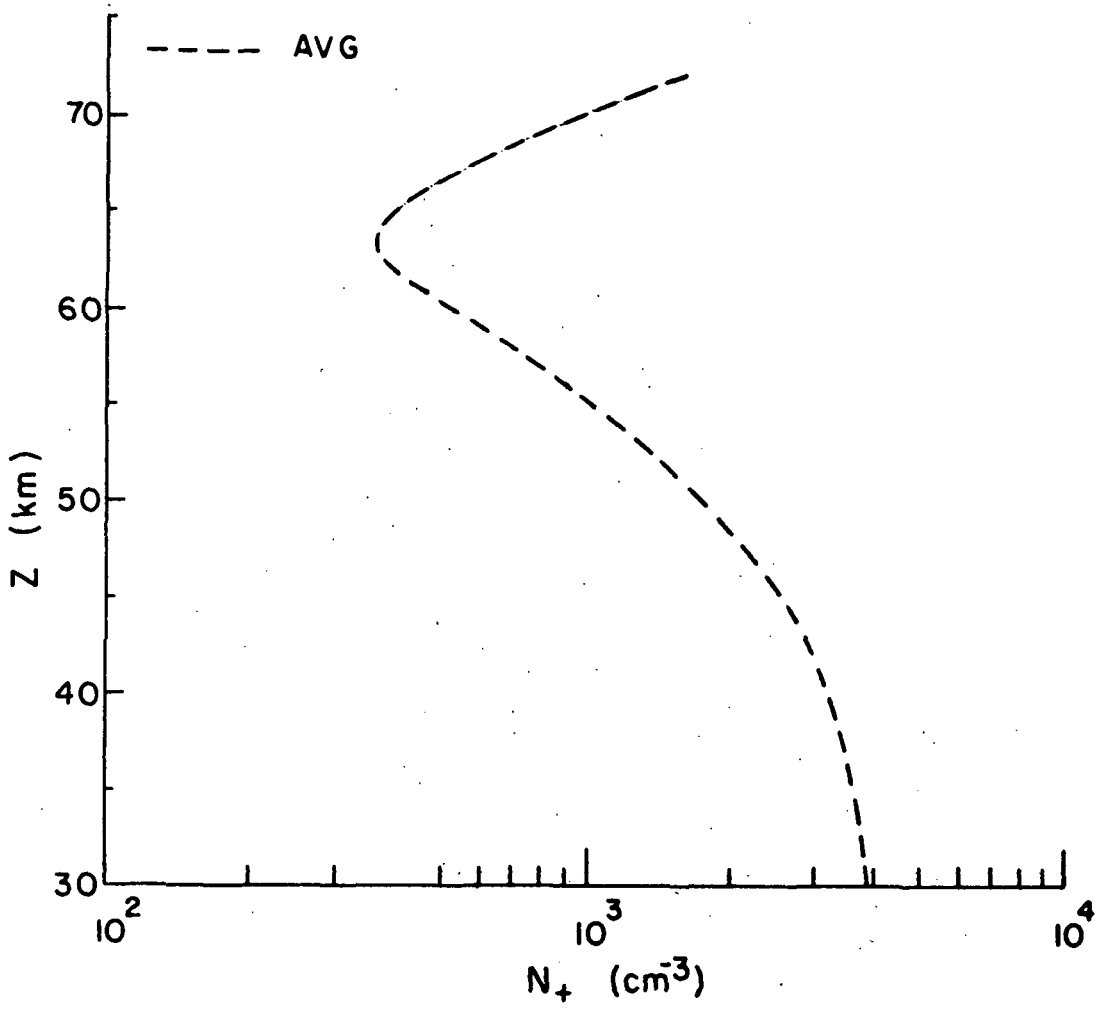

Figure 13. The Average Positive Ion Density Profile Computed from CIRA 65

Since $\mu_e >> \mu_-$, (14) can be written

$$N_e \simeq \frac{\sigma_- - N_+ e\mu_-}{e\mu_e} \qquad (15)$$

Because electron drift velocity is not a linear function of the applied electric field, electron mobility is difficult to define. Electron mobility can be estimated as a function of E/P (Mitchell and Hale, 1972), however, this procedure introduces some uncertainty in the absolute values of electron densities. Since all data were reduced in a consistent manner, a greater level of confidence is placed in electron densities considered relative to each other than in their absolute values.

Electron densities are calculated from (15), where μ_{o-} is assumed to be 2.3 $cm^2V^{-1}sec^{-1}$ (Loeb, 1955; Cole and Pierce, 1965) and all meteorological data are taken from CIRA 65. At altitudes between 45 and 63 Km, where $\sigma_- >> \sigma_+$, (15) reduces to

$$N_e \simeq \frac{\sigma_-}{e\mu_e} \qquad (16)$$

Smoothed curves of electron densities as function of altitude are presented in Figures 14 and 15.

3.3 Negative Ion Densities

From Figures 11 through 15 it can be seen that $N_+ >> N_e$ between 30 and 63 Km. Combining this observation with the requirement for charge neutrality given by (13) yields

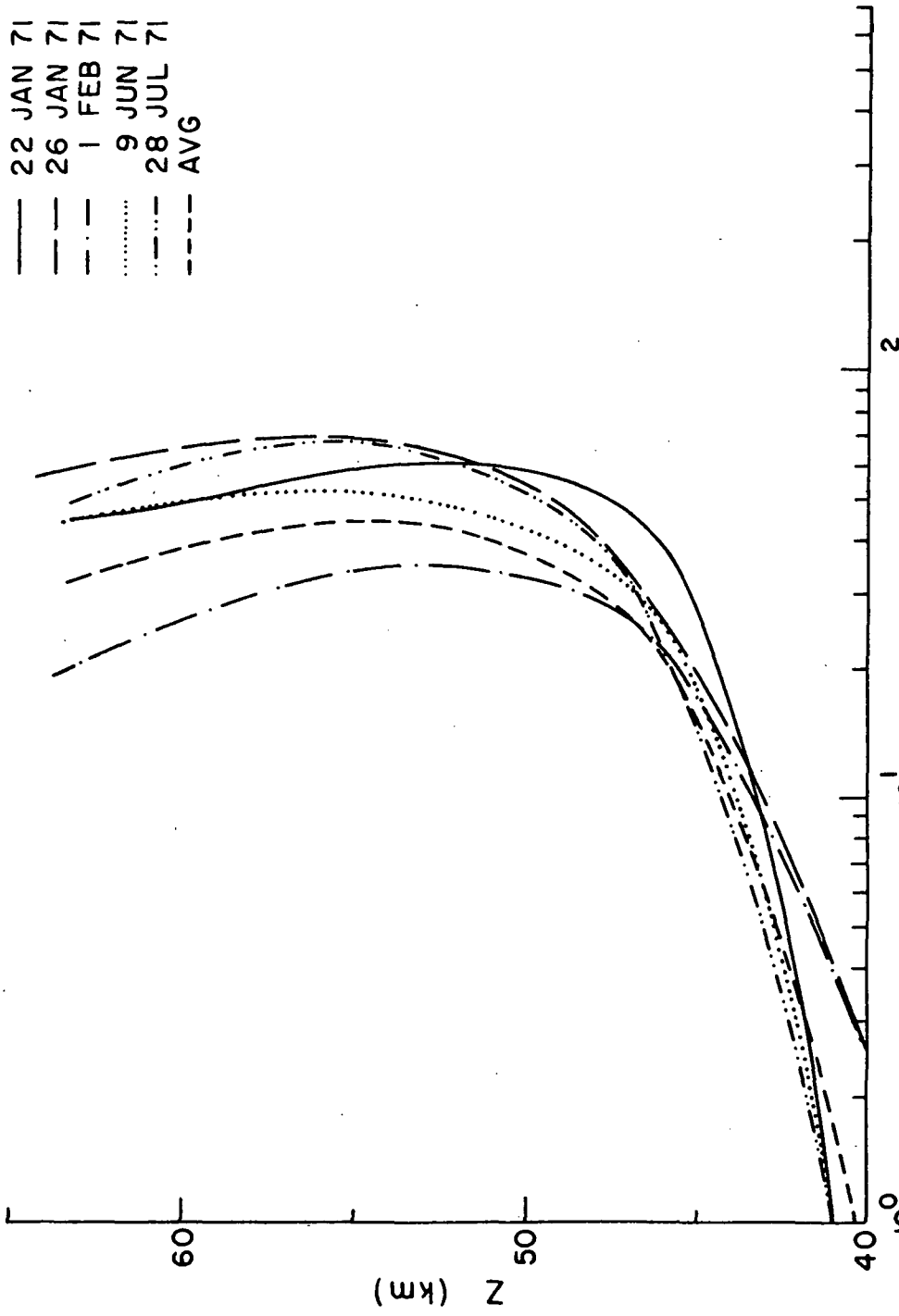

Figure 14. Smoothed Electron Density Profiles

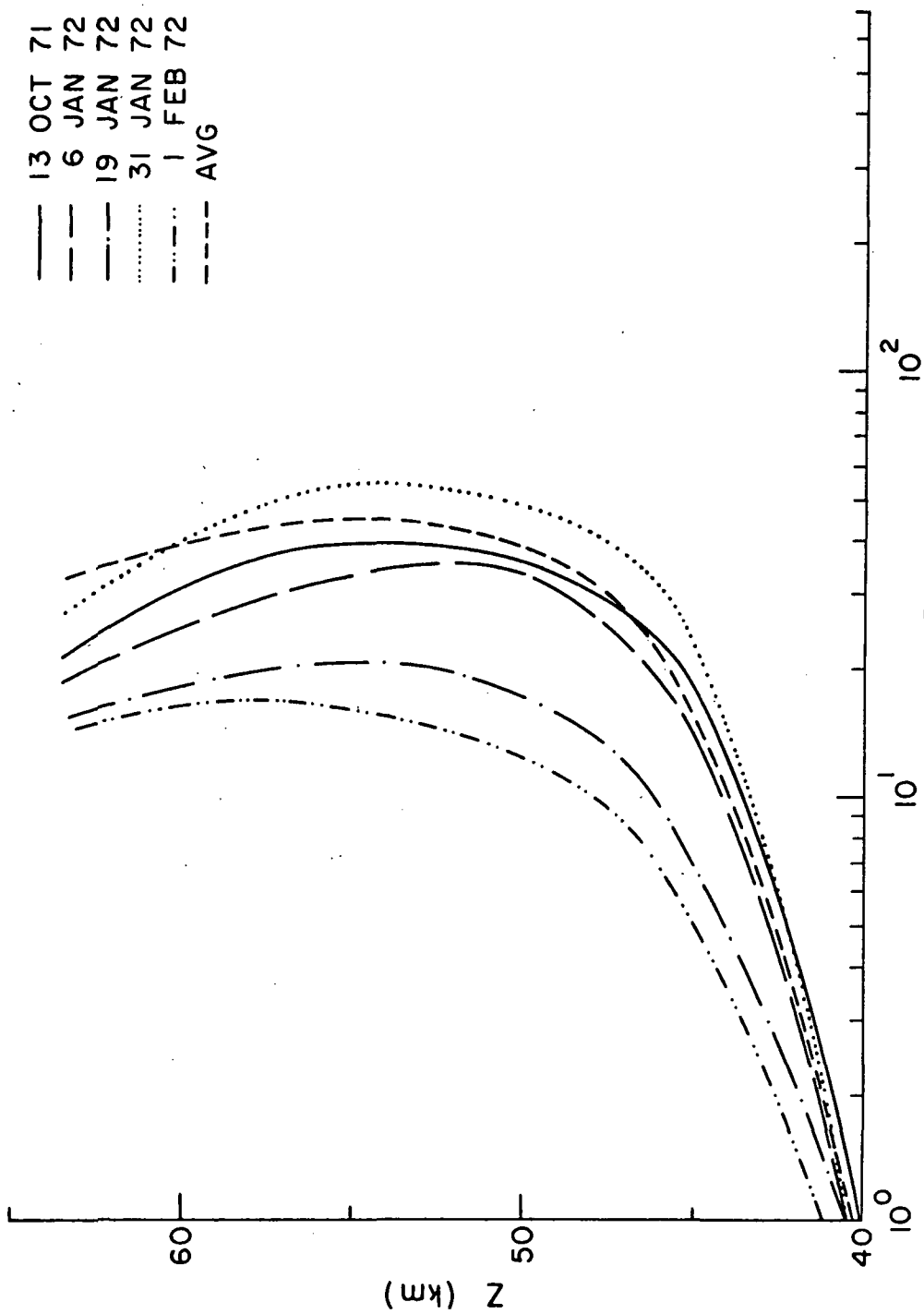

Figure 15. Smoothed Electron Density Profiles

$$N_- \simeq N_+ \qquad (17)$$

within this altitude range. Thus Figures 11 and 12 are also representative of N_- profiles.

CHAPTER IV

DATA ANALYSIS

4.1 General Procedure

Correlations among positive and negative conductivities, meteorological parameters and HF radio wave absorption are obtained as functions of altitude. Correlation coefficients (r) are calculated between each pair of parameters at altitudes for which 10 data points are available (one point from each launch). Table 5 lists the height ranges within which correlation coefficients are computed, and r values are given at 5 Km intervals in the Appendix. Parameters that are well correlated with one another are analyzed in the following sections.

4.2 Positive Conductivity

4.2.1 Positive and Negative Conductivities

Below about 40 Km the two conductivities are approximately equal (see Figures 3 and 4), indicating an absence of electrons. However, they diverge rapidly from each other above 40 Km, and their r values drop quickly with increasing altitude, becoming less than 0.65 above 46 Km (see Appendix).

4.2.2 Positive Conductivity and Temperature

Positive conductivity correlates very well with temperature, the strongest correlations ($r > 0.90$)

Table 5

Height Ranges within which Correlation Coefficients are Determined

	σ_+	σ_-	T	ρ
σ_+	xx	30-63 Km	30-58 Km	30-58 Km
σ_-	30-63 Km	xx	30-58 Km	30-58 Km
T	30-58 Km	30-58 Km	xx	30-58 Km
L	30-63 Km	30-63 Km	30-58 Km	30-58 Km

occurring between 48 and 58 Km. The r values remain greater than 0.70 at lower altitudes until a relatively sharp drop begins at 32 Km. The correlation coefficients between σ_+ and T are plotted as functions of altitude in Figure 16.

Relationships of the form

$$\sigma_+ = a(z)T - b_+(z) \tag{18}$$

are obtained at the various altitudes by the least squares method. Graphs of such functions are given for heights of 35, 45 and 55 Km in Figures 17, 18 and 19 respectively.

Between 33 and 58 Km, where $r \geq 0.75$, the slopes (a(z)) are proportional to the intercepts ($b_+(z)$) in such a manner that

$$\frac{a(z)}{b_+(z)} = a_+(z) \tag{19}$$

where $a_+(z)$ is a weak function of altitude. Substituting (19) into (18) gives

$$\sigma_+ = b_+(z)(a_+(z)T - 1.0) \tag{20}$$

where $b_+(z)$ and $a_+(z)$ are given in Figures 20 and 21 respectively. Assuming $b_+(z)$ to be a linear function of altitude yields (see Figure 20)

$$b_+(z) = 2.67Z - 82.3 \tag{21}$$

within the height range being considered.

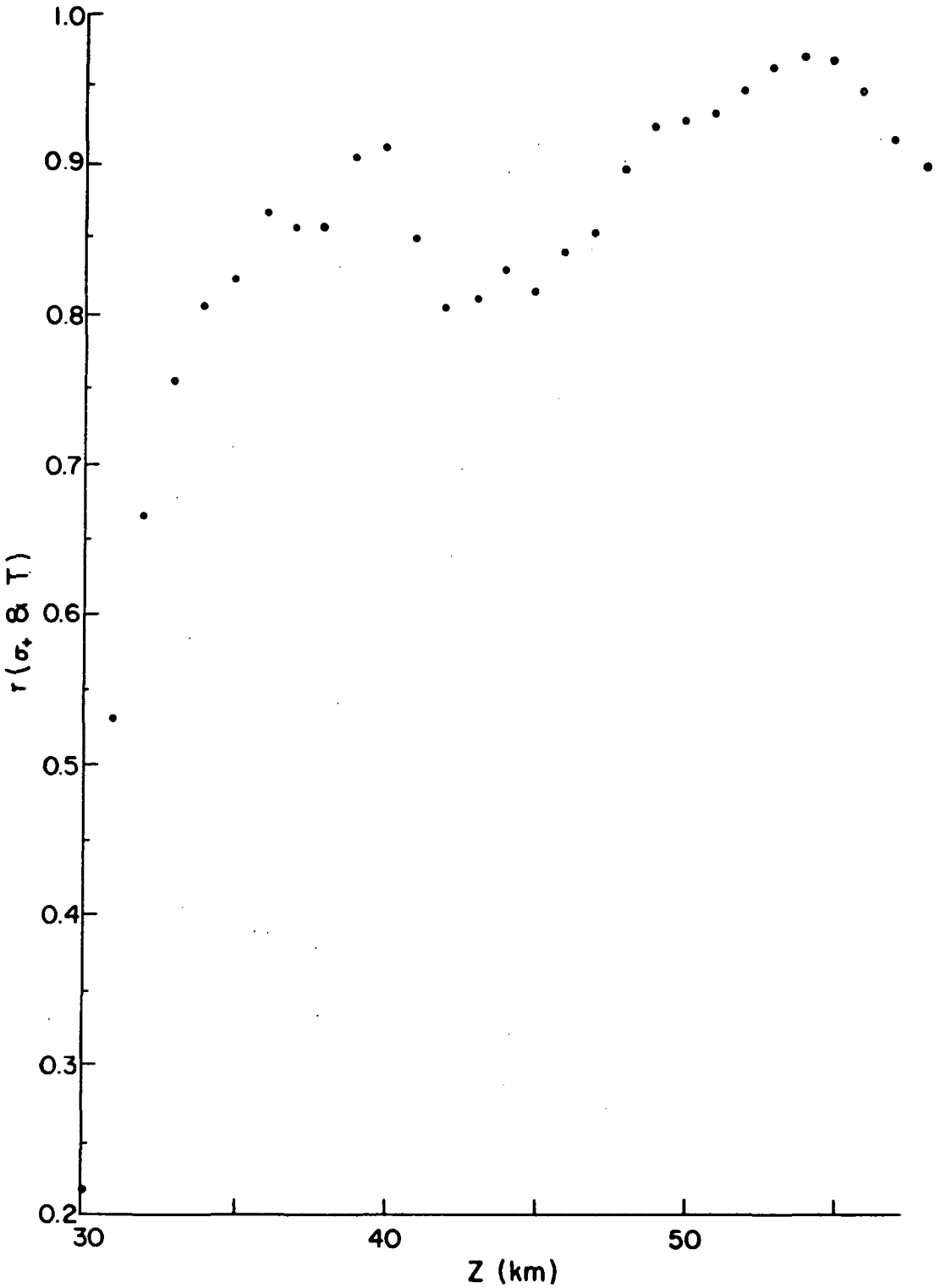

Figure 16. Correlation Coefficients (σ+ and T) vs Altitude

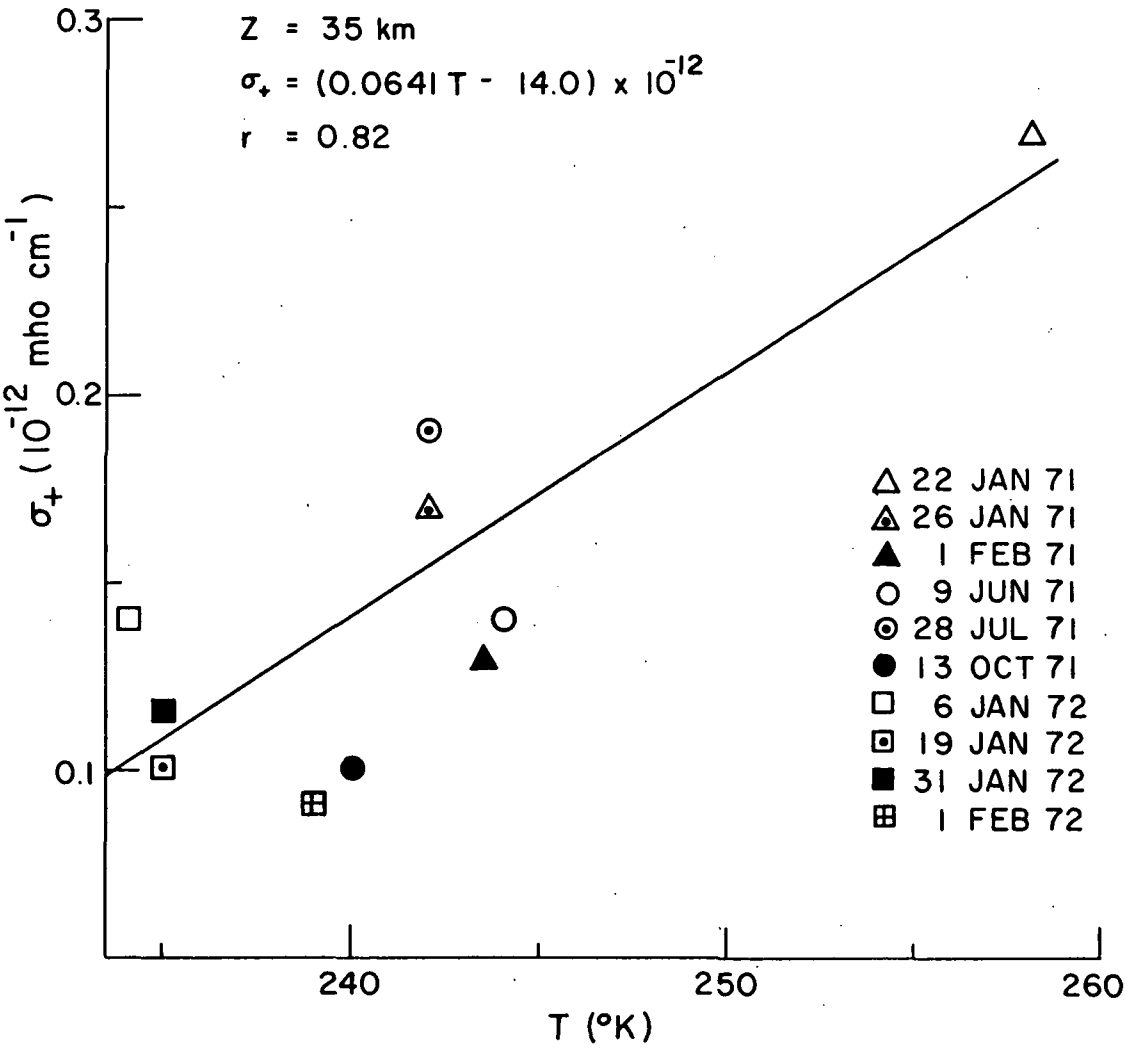

Figure 17. Positive Conductivity vs Temperature (35 Km)

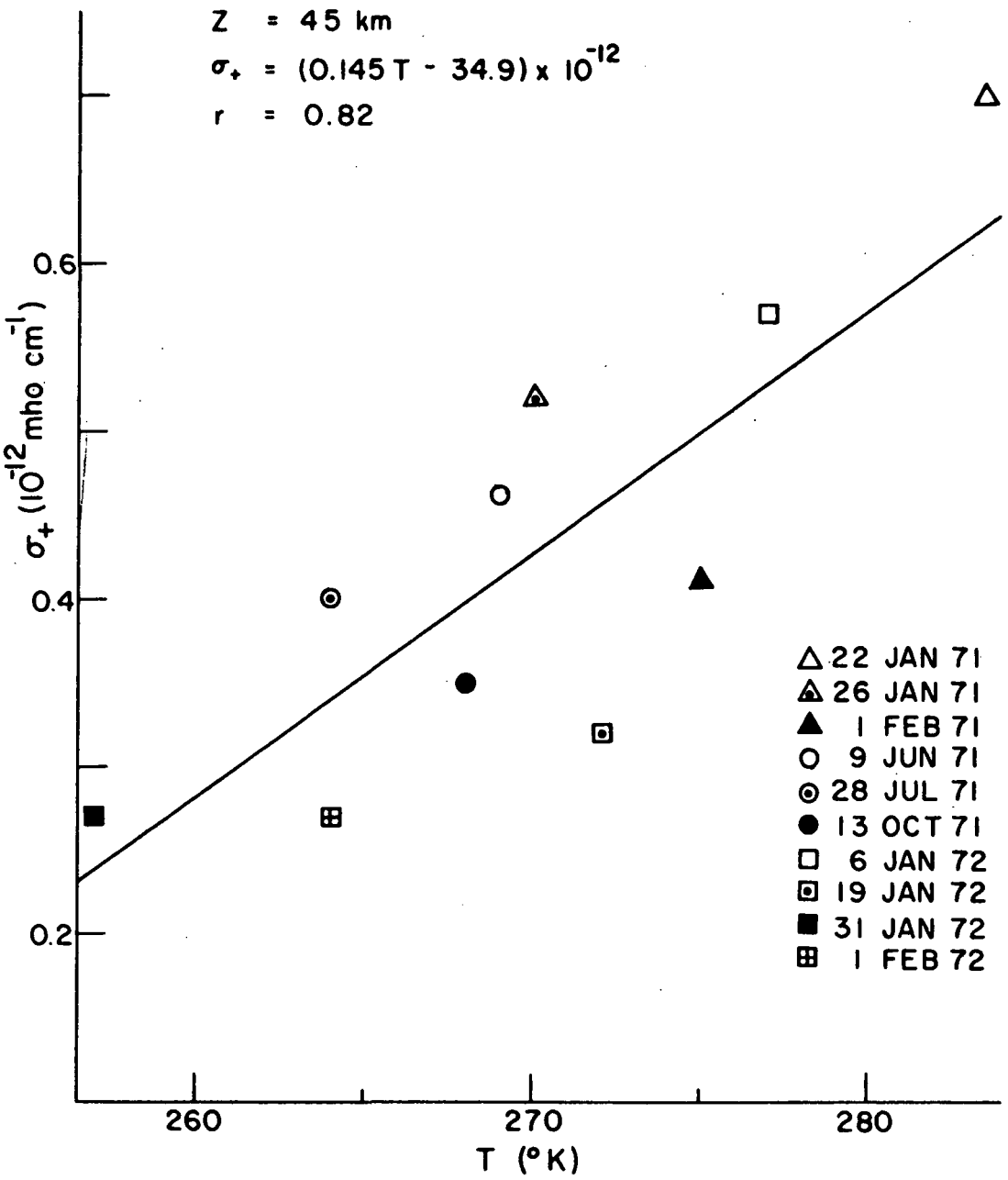

Figure 18. Positive Conductivity vs Temperature (45 Km)

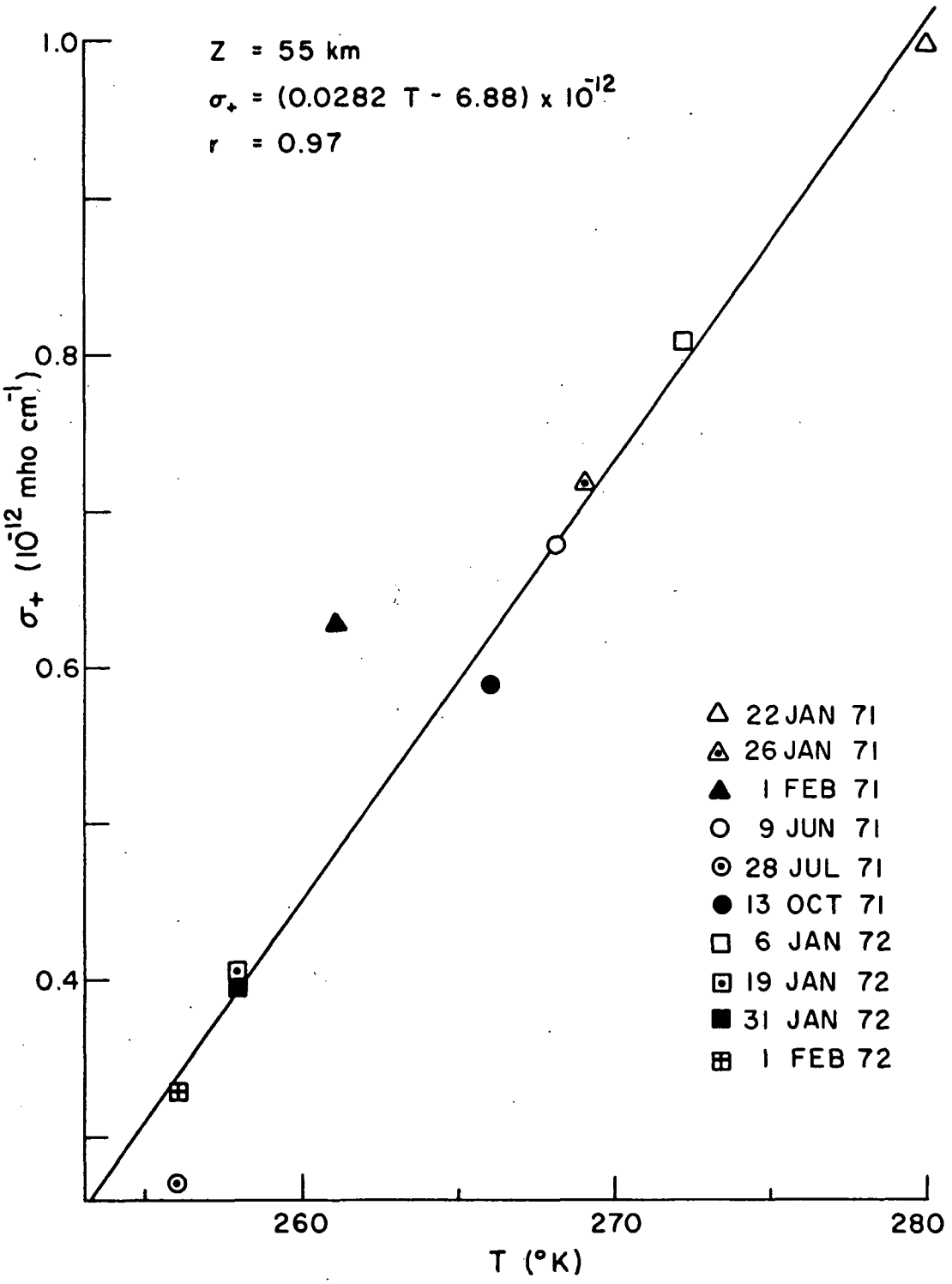

Figure 19. Positive Conductivity vs Temperature (55 Km)

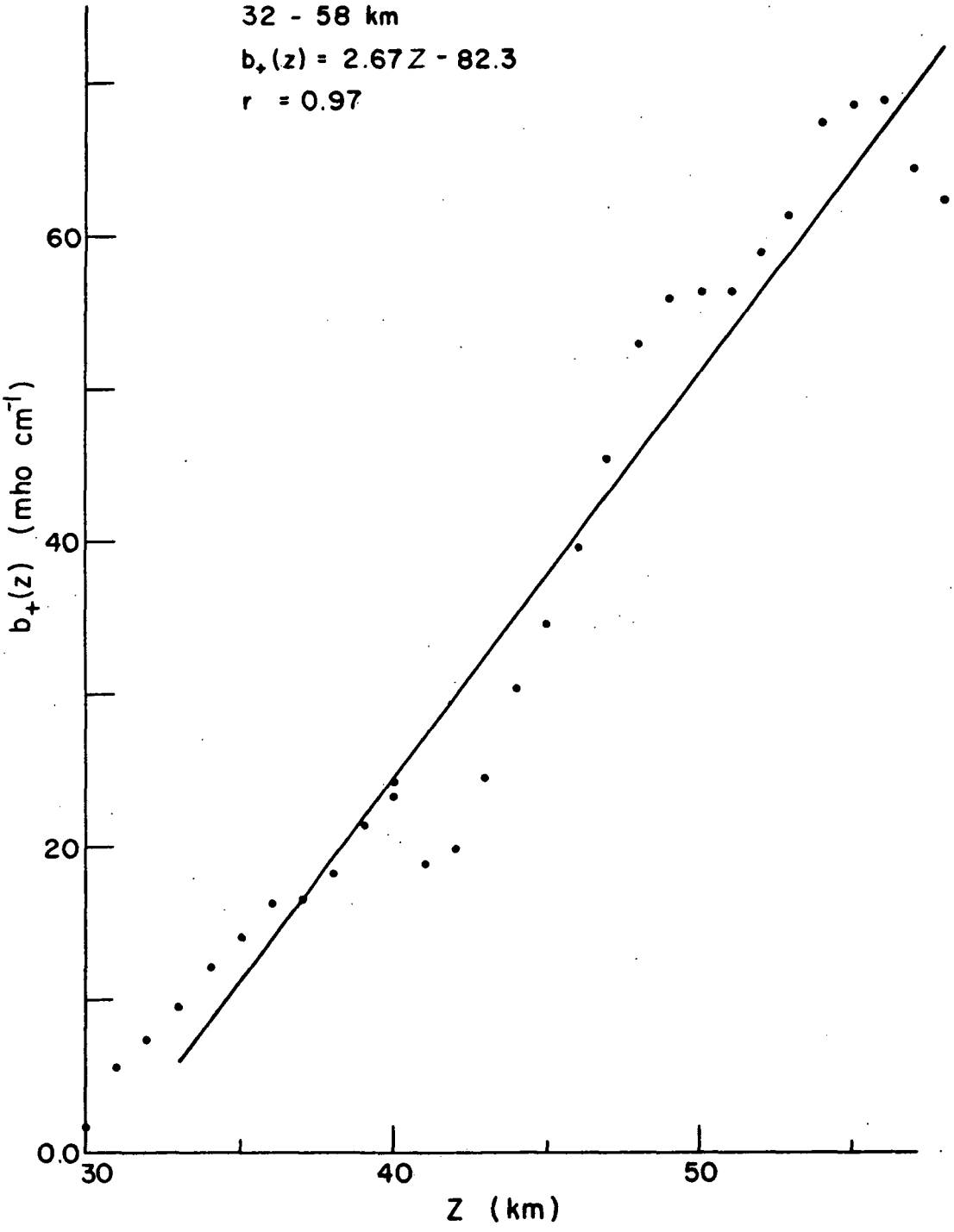

Figure 20. Intercept ($b_+(z)$) vs Altitude

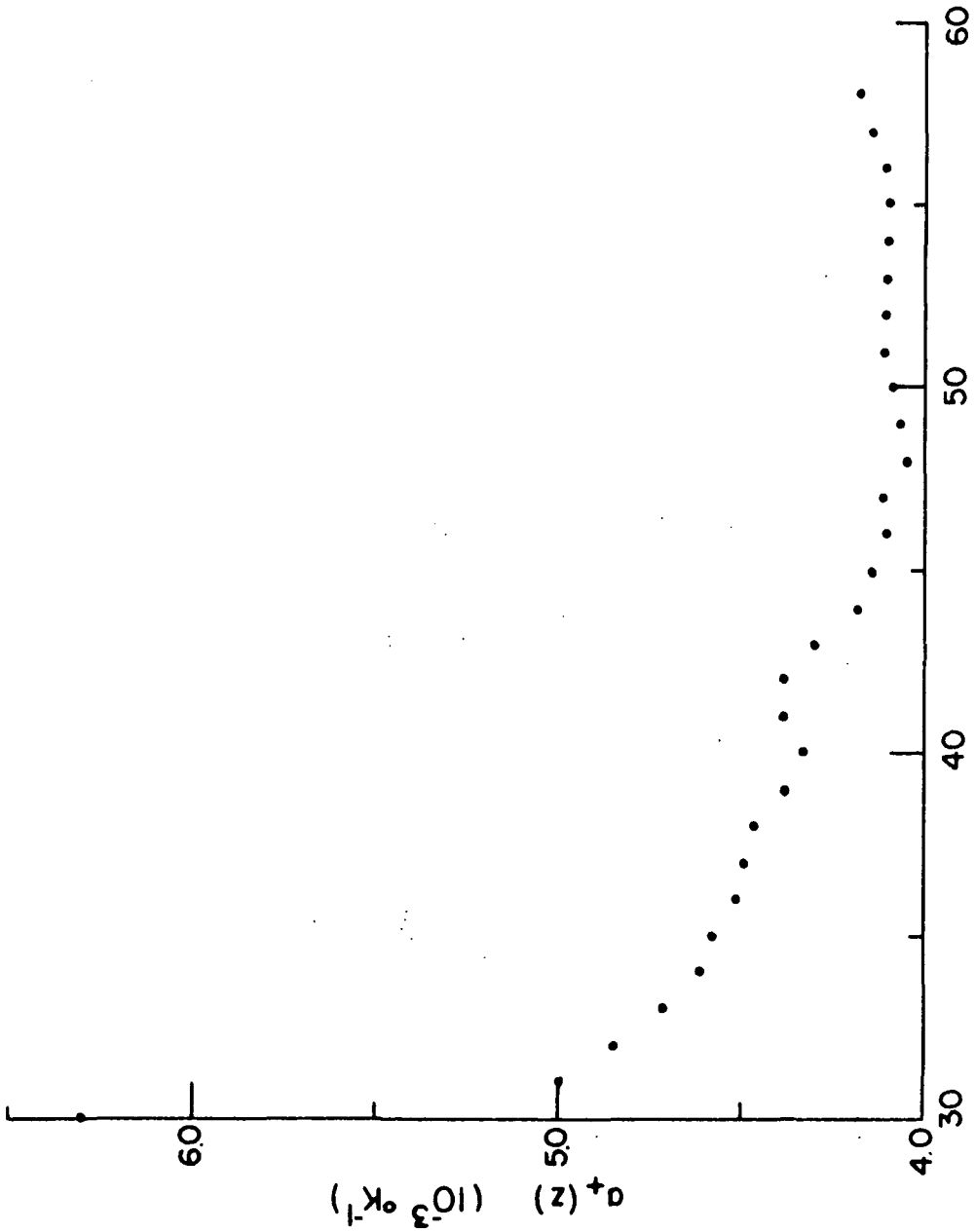

Figure 21. Slope-Intercept Ratio ($a_+(z)$) vs Altitude

Figure 21 indicates that $a_+(z)$ is virtually independent of altitude above 43 Km, while below this level it varies linearly with height. Such behavior is strikingly similar to that exhibited by the temperature profiles in Figures 6 and 7, suggesting that $a_+(z)$ may be replaced by $a_+(T)$ in (20), that is

$$\sigma_+ = b_+(z)(a_+(T)T - 1.0) \tag{22}$$

Figure 22, which plots $a_+(T)$ as a function of the average temperatures given in Figures 6 and 7, indicates that (22) can be expressed as

$$\sigma_+ = 4.12\text{x}10^{-3} b_+(z)((-2.77\text{x}10^{-3}T+1.78)T-243) \tag{23}$$

between 33 and 43 Km, and as

$$\sigma_+ = 4.12\text{x}10^{-3} b_+(z)(T - 243) \tag{24}$$

from 44 to 58 Km.

The temperature coefficient for positive conductivity (σ_{+T}) is defined by

$$\sigma_{+T} = \frac{1}{\sigma_+}\frac{\partial \sigma_+}{\partial T} \tag{25}$$

and, from (22) may be written as

$$\sigma_{+T} = \frac{a_+(T) + T\,\dfrac{\partial a_+(T)}{\partial T}}{a_+(T)T - 1.0} \tag{26}$$

Values for σ_{+T} are given at 5 Km intervals in Table 6, where the required temperatures are obtained from the average curve in Figures 6 and 7. The values found in

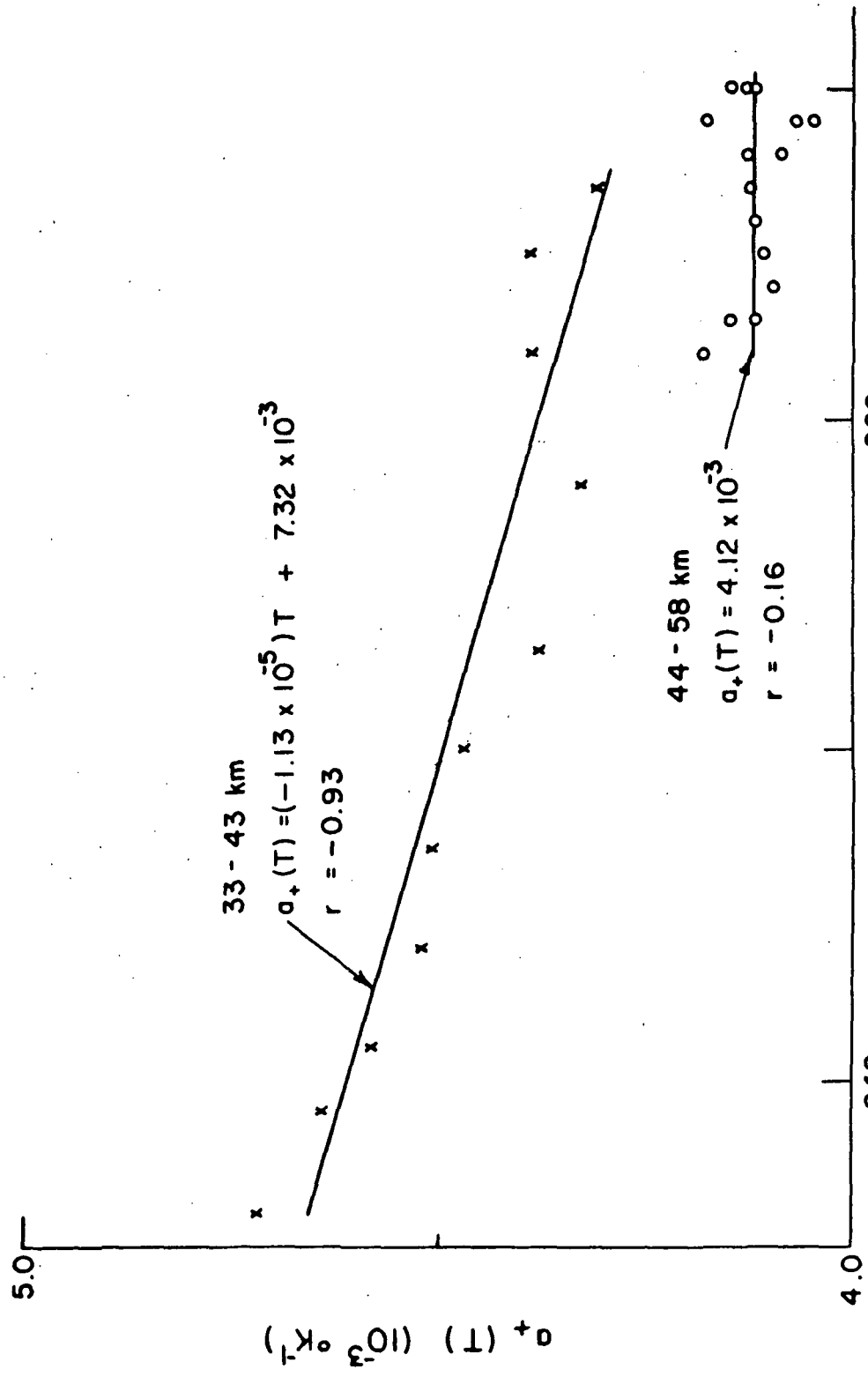

Figure 22. Slope-Intercept Ratio ($a_+(T)$) vs Temperature

Table 6

Temperature Coefficients for
Positive Conductivity

Height (K_m)	Temperature Coefficient (% $^oK^{-1}$)
55	4.6
50	4.1
45	3.7
40	1.1
35	1.7

Table 6 are up to an order of magnitude greater than can be expected to result solely from the temperature dependence of the mobility of a single species, as inferred from (10).

From (9), these unexpectedly large values of σ_{+T} imply either that N_+ is a function of T or that (10) does not describe $\mu_+(T)$ within this altitude range. The former seems less probable because N_+ would be expected to correlate well with N_e, but no such corresponding correlation between σ_+ and σ_- is observed (except at altitudes where $N_e \simeq 0$). The latter could be due to the rapid variations with temperature in the size of the hydrated ions expected to form at these altitudes (Narcisi and Bailey, 1965). In this case, the large values computed for σ_{+T} would be due to the effect on μ_+ of variations in the amount of water clustering (Kebarle, Searles, Zolla, Scarborough and Arshadi, 1967). This effect does not appear to be uniform throughout the 33-58 Km region (see Figure 22 and Table 6). If this speculative reasoning is valid, then the assumptions and expressions from which (11) was derived must be re-evaluated.

4.3 High Frequency Radio Wave Absorption and Negative Conductivity

4.3.1 General Discussion

Since absorption occurs almost entirely above 60 Km, where ionization production is principally dependent on solar UV radiation (see Section 2.3.1), it exhibits the strong diurnal variations seen in Figures 9 and 10. In contrast, negative conductivity is determined below 65 Km,

where ionization production is primarily due to galactic cosmic rays, and therefore exhibits relatively little variability over a one year period of measurement. Thus, excepting the small overlap between 60 and 65 Km, absorption and negative conductivity data are measured in regions having vastly different production sources.

However, both relative absorption and negative conductivity are expected to be proportional to electron density at their respective levels. Therefore, comparisons of these two parameters should make it possible to determine if electron densities at the separate levels are coupled. Such comparisons are made for the L values defined in Section 2.3.2, and the results are discussed in the following sections.

4.3.2 Relative Noon Absorption (L_n) and Negative Conductivity

Correlation coefficients between relative noon absorption and negative conductivities at 62 and 63 Km are greater than 0.90. As the altitudes from which σ_- data are obtained decrease, the correlation coefficients between L_n and σ_- also decrease, dropping below 0.70 at 52 Km. Figure 23 plots the correlation coefficients between L_n and σ_- as functions of the altitude of σ_-. The r values between these two parameters appear to be independent of the season and solar zenith angle at which they are measured (see Tables 1 and 4), and also of the blunt probe launch time (see Table 1).

The good correlations between L_n and σ_- imply that coupling does exist between electron densities at the separate levels. Since ionization production differs greatly within the two regions, it can be speculated that the day-to-day variations in L_n are due to changing atmospheric conditions affecting electron loss rate, and not to variations in production. Furthermore, the large distances from the launch facilities to the mid-points of their absorption paths (see Section 2.3.1) suggest that the atmospheric conditions which affect electron loss rate extend over a large geographical area.

Expressions of the form

$$L_n = a_-(z)\sigma_- + b_-(z) \qquad (27)$$

are determined in a manner analogous to that described in the case of (18). Graphs of L_n as functions of σ_- are given in Figures 24, 25 and 26 for heights of 50, 55 and 60 Km respectively, while plots of $a_-(z)$ and $b_-(z)$ as functions of altitude are shown in Figures 27 and 28. These latter figures indicate that $a_-(z)$ is an exponentially decreasing function of altitude, and that $b_-(z)$ is essentially independent of height. Between 54 and 63 Km, where $r \geq 0.74$, $a_-(z)$ can be approximated by a linear function of altitude. Within this height range (27) becomes (see Figures 27 and 28)

$$L_n = (-6.55\times10^{-3}Z + 0.468)\sigma_- + 18.5 \qquad (28)$$

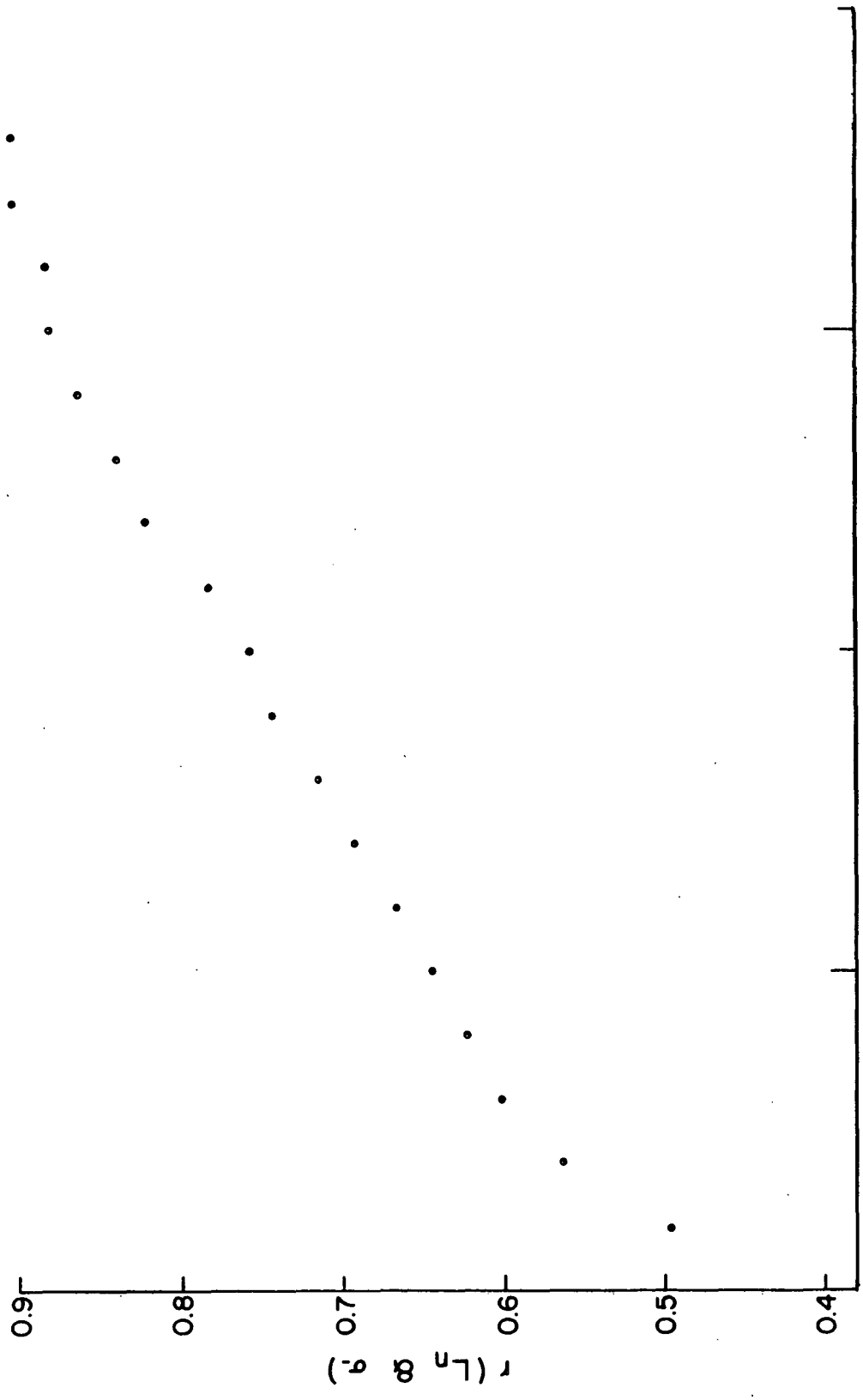

Figure 23. Correlation Coefficients (L_n and σ-) vs Altitude

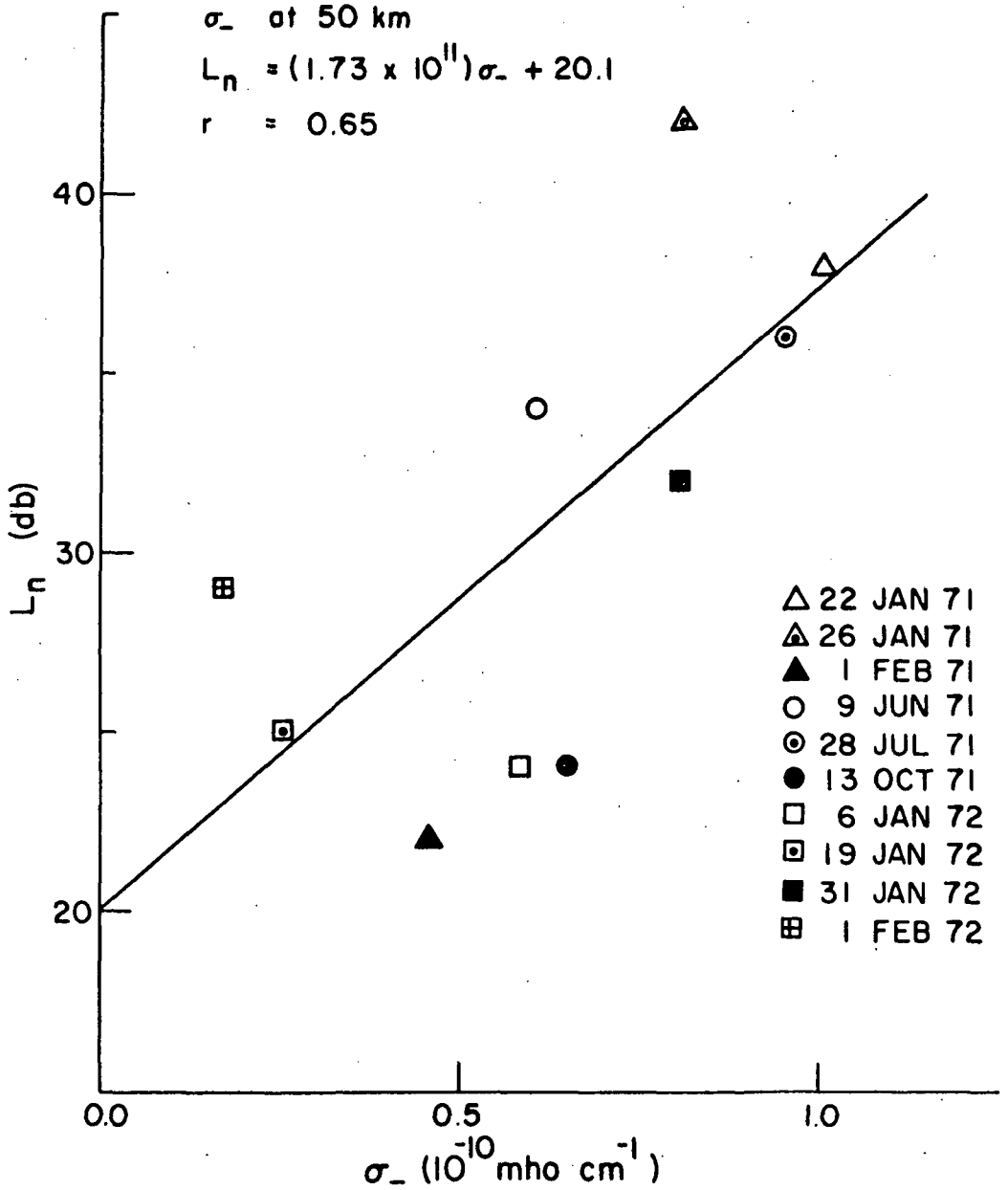

Figure 24. Relative Noon Absorption vs Negative Conductivity at 50 Km

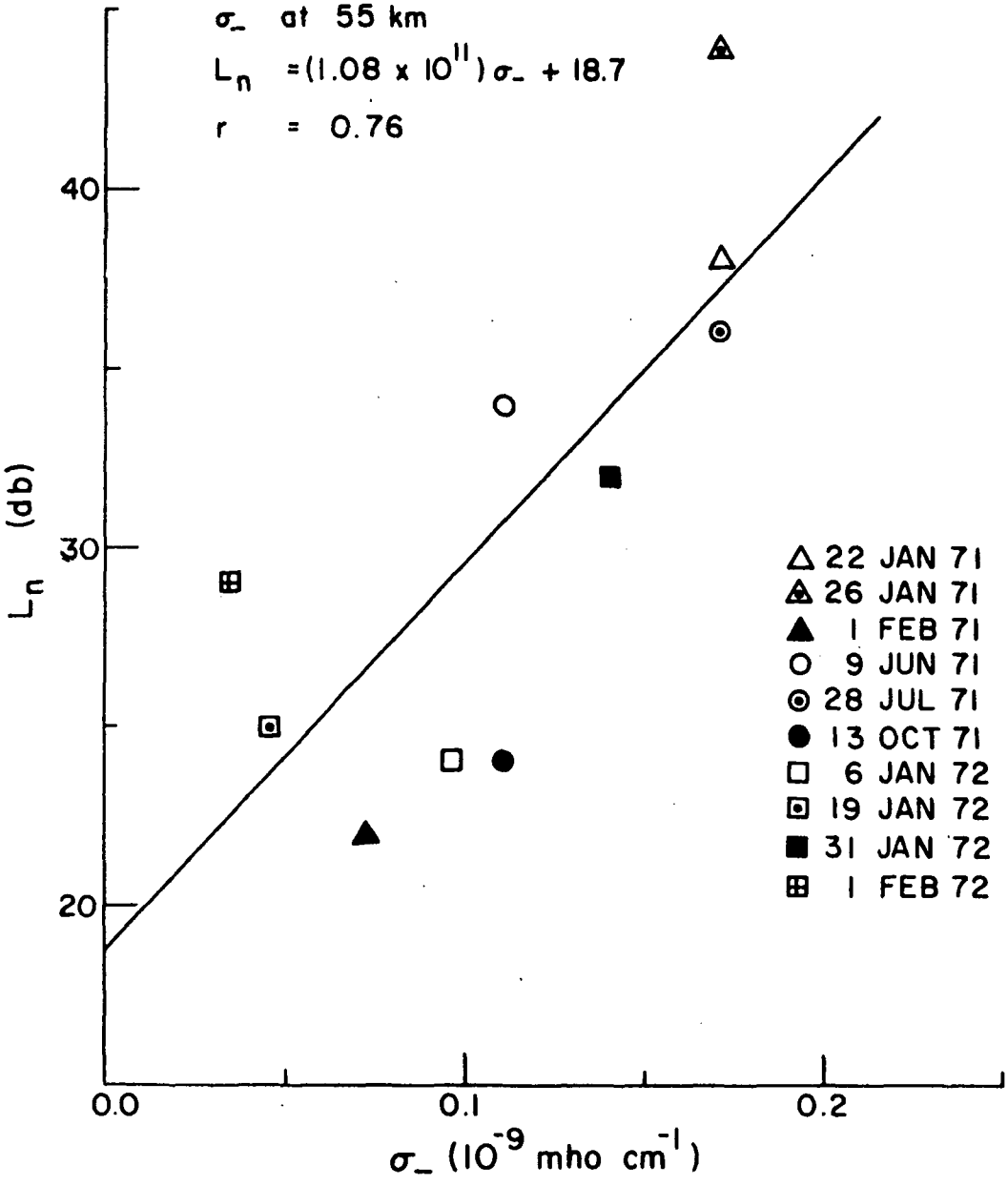

Figure 25. Relative Noon Absorption vs Negative Conductivity at 55 Km

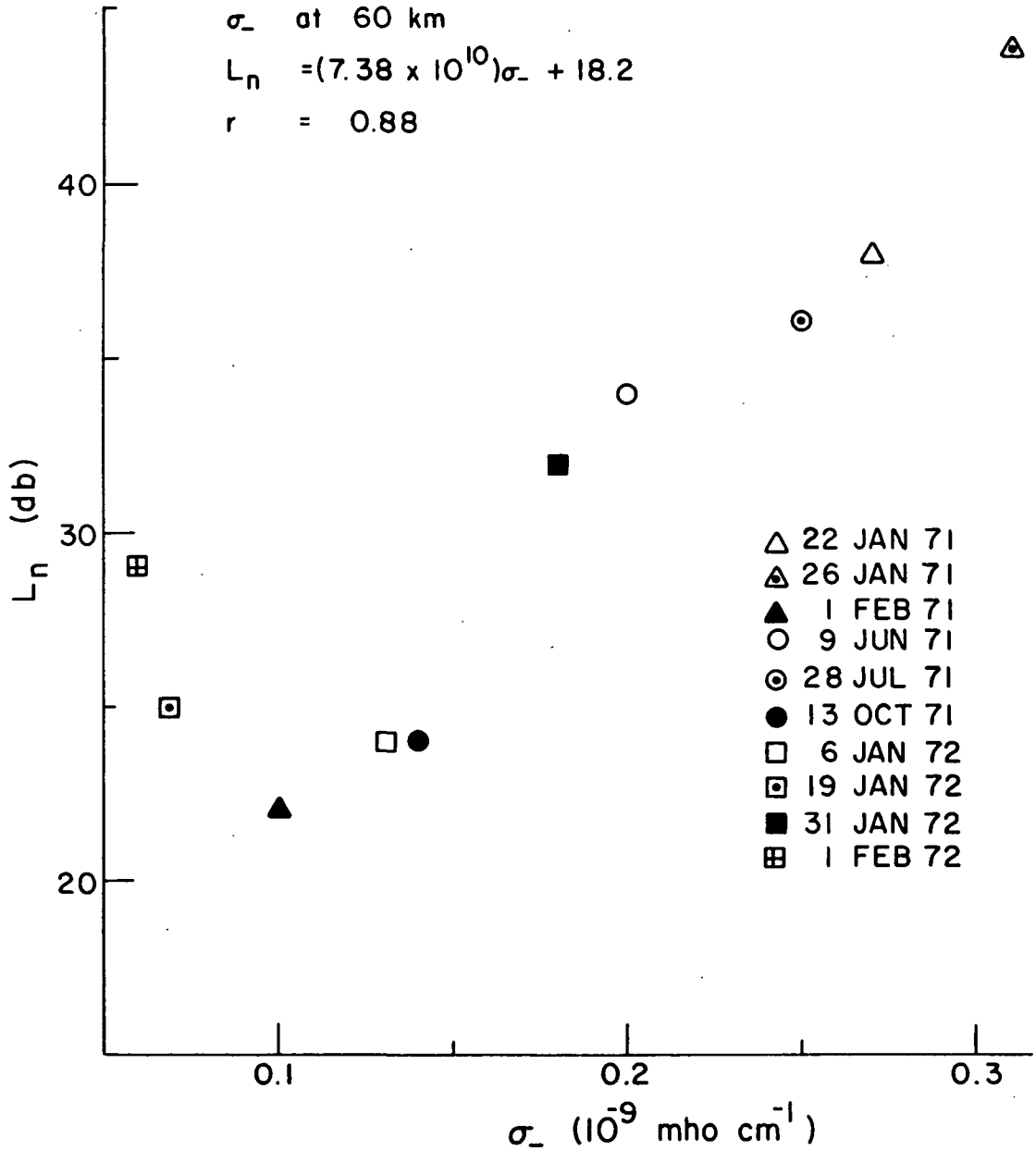

Figure 26. Relative Noon Absorption vs Negative Conductivity at 60 Km

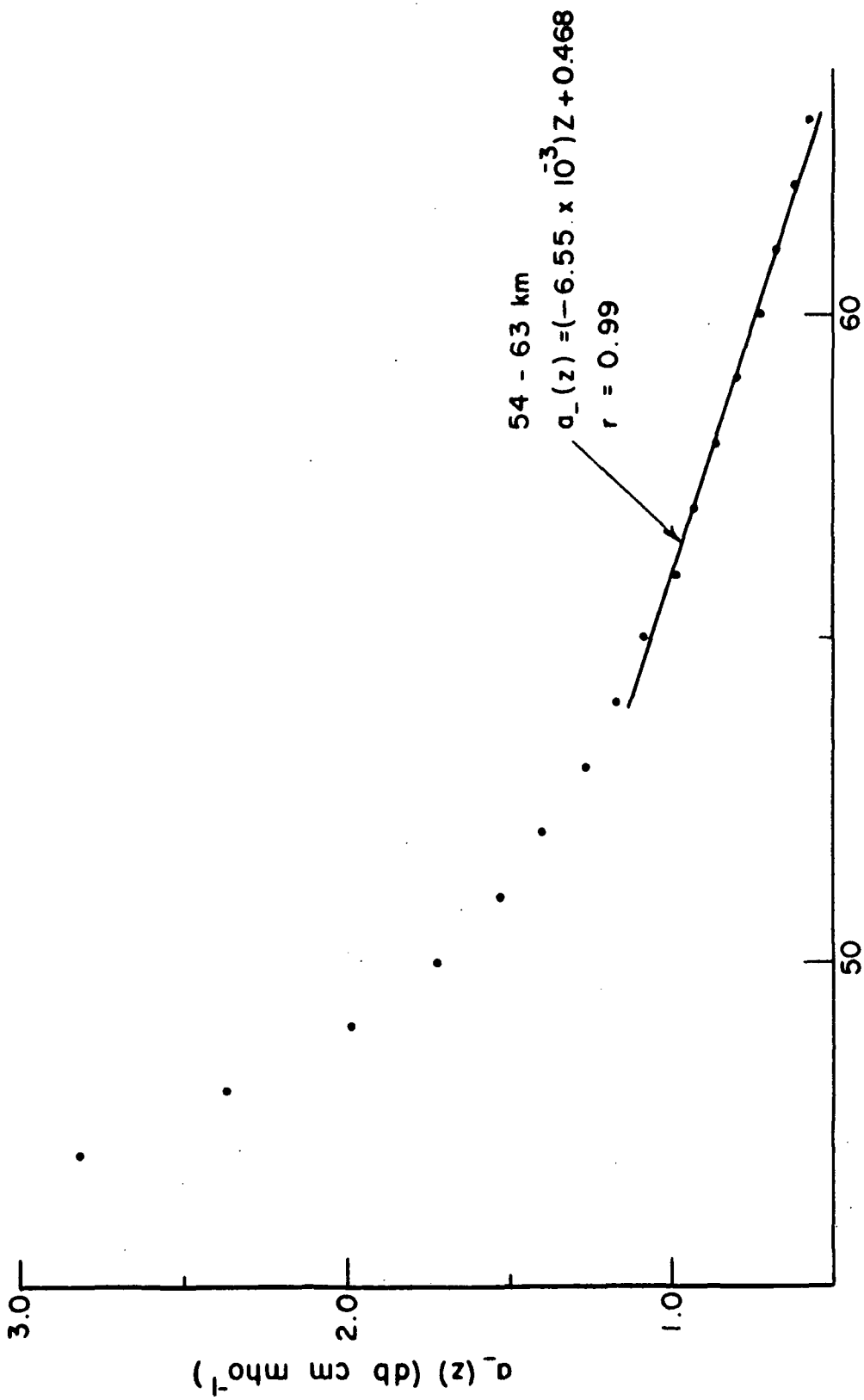

Figure 27. Slope ($a_{-}(z)$) vs Altitude

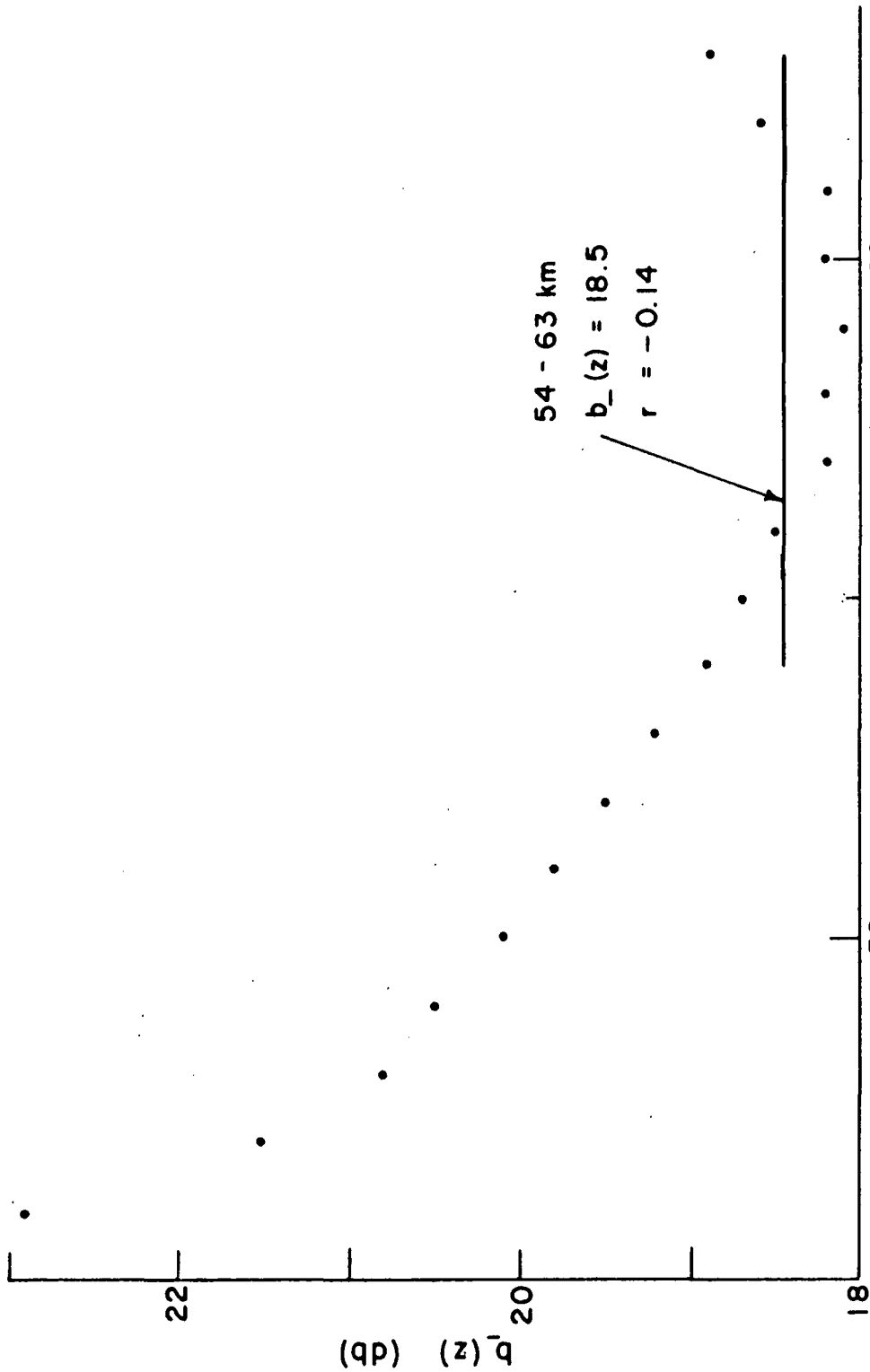

Figure 28. Intercept (b_(z)) vs Altitude

suggesting that a significant percentage of L_n is independent of σ_-, and therefore, from (16), of N_e. This percentage ranges from 42 per cent on January 26, 1971, to 84 per cent on February 1, 1971. An explanation of this result requires considerations beyond the scope of this work.

High correlation coefficients between L_n and σ_- are obtained despite the February 1, 1972 data, which exhibit negative conductivity values that are too low for their corresponding relative absorption (see Figures 25 and 26). This fact is discussed further in the next section.

4.3.3 Relative Absorption at a Given Solar Zenith Angle of 60° (L_χ) and Negative Conductivity

Correlation coefficients between relative absorption at a zenith angle of 60° and negative conductivity are not as high as those observed between L_n and σ_- (see Appendix). The reason for the poorer correlations found in this case can be inferred from Figures 29 and 30, which respectively give $L_{\chi AM}$ and $L_{\chi PM}$ as functions of σ_- at 60 Km. In both morning and afternoon cases, the two summer launch data exhibit L_χ values which are too low for their corresponding negative conductivities. This observation suggests seasonal variations in the quantity L_χ.

Figures 29 and 30 also indicate that while the February 1, 1972 $L_{\chi AM}$ value agrees with its corresponding σ_- value, the $L_{\chi PM}$ value for this date does not. The seemingly uncharacteristic behavior of the February 1, 1972

data can be seen in Figures 24, 25, 26 and 30, but not in Figure 29. This suggests that the coupling between the two levels discussed in the previous section may have broken down shortly after the $L_{\chi AM}$ measurement (1012 MST - see Figures 8 and 10).

4.3.4 Relative Absorption at the Time of Blunt Probe Launch (L_p) and Negative Conductivity

Relative absorption determined at the time of blunt probe launch is poorly correlated with negative conductivity (see Appendix). This is not surprising since the payload launches occurred over a wide variety of times, zenith angles and seasons (see Table 1). A plot of L_p as a function of $\sigma-$ at 60 Km is shown in Figure 31.

Thus negative conductivity measurements appear to be good indicators of L_n (see Section 4.3.2), but not necessarily of L_p. For example, all three morning launches (see Table 1) exhibited $\sigma-$ values corresponding to L_n, suggesting that atmospheric conditions affecting the relative noon absorption are set early in the day and are subject to little subsequent diurnal variation. If this is the case, it then becomes possible to speculate that relative noon absorption can be predicted from an early morning measurement of the negative conductivity at about 60 Km.

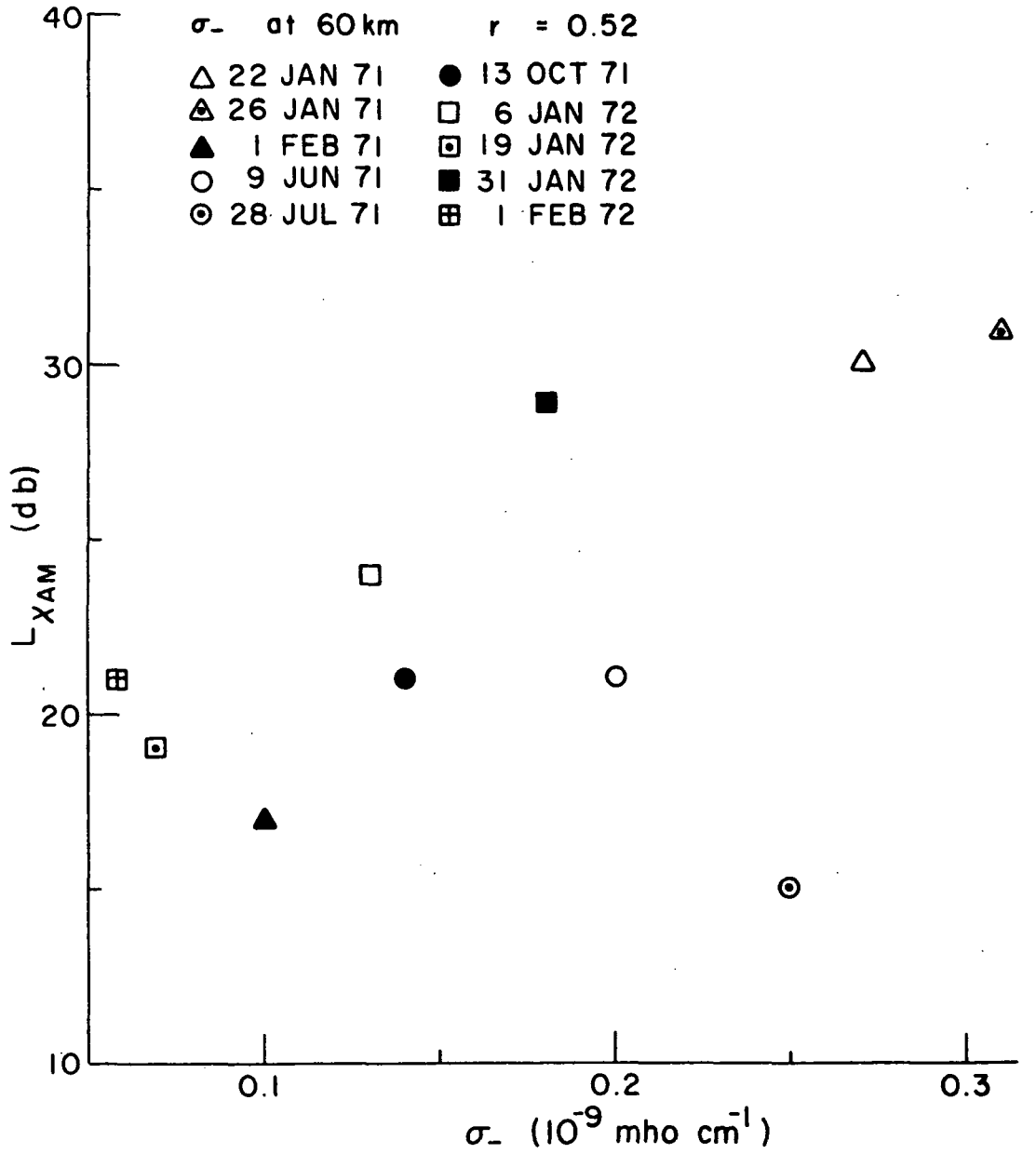

Figure 29. Relative Absorption for a Zenith Angle of 60° (AM) vs Negative Conductivity at 60 Km

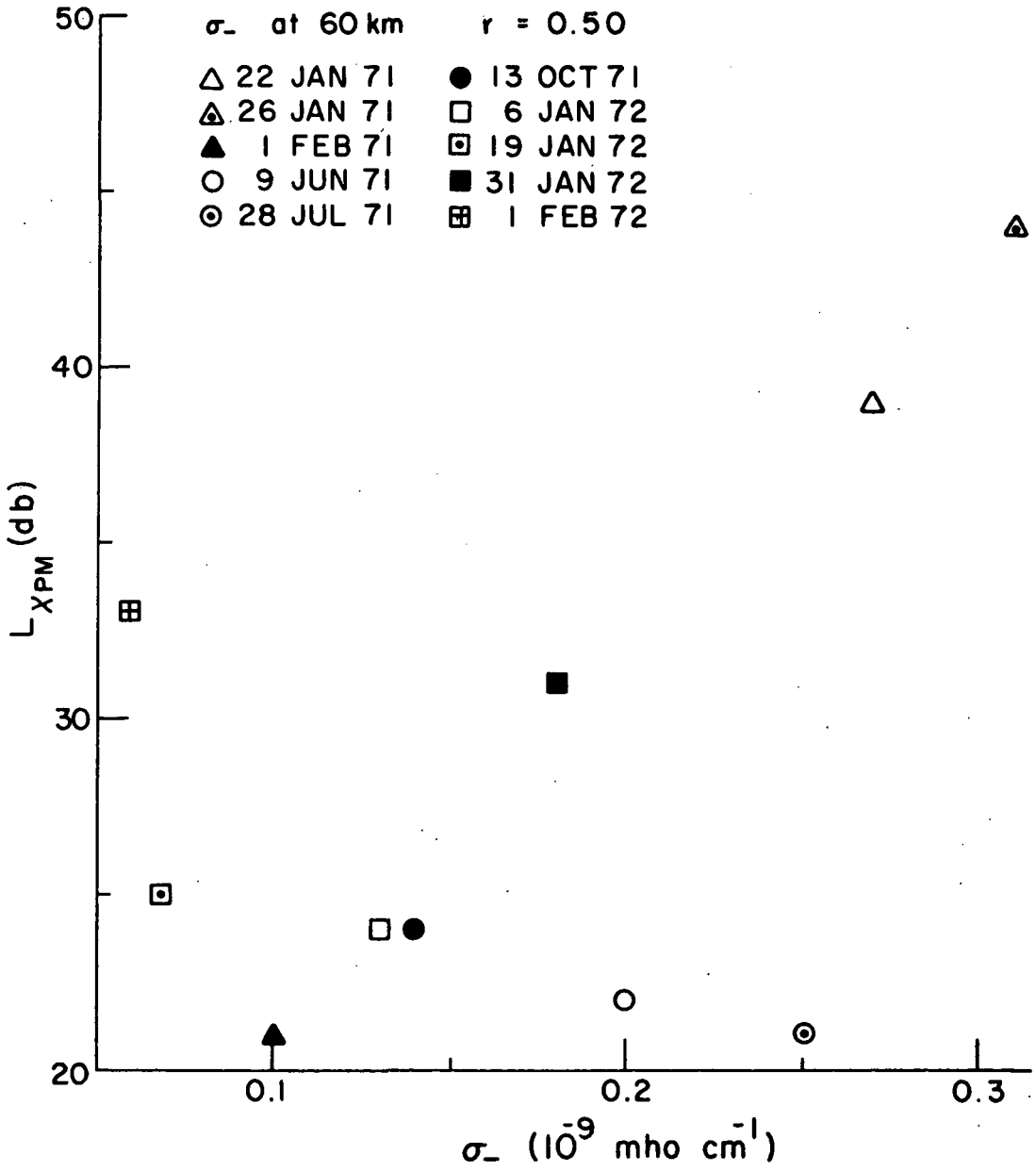

Figure 30. Relative Absorption for a Zenith Angle of 60° (PM) vs Negative Conductivity at 60 Km

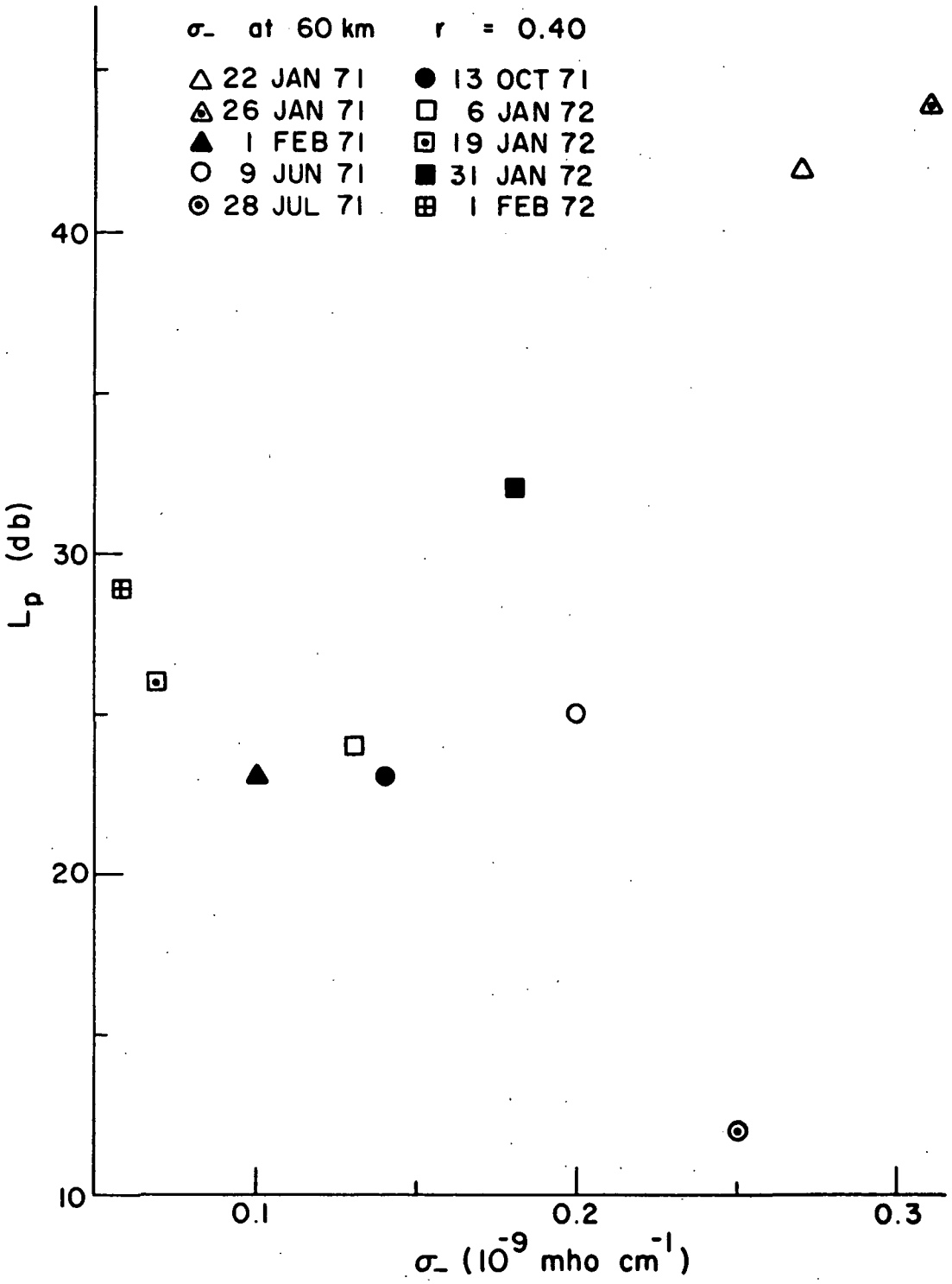

Figure 31. Relative Absorption at the Time of Blunt Probe Launch vs Negative Conductivity at 60 Km

CHAPTER V

CONCLUSION

5.1 Summary of Results

Electrical conductivities, measured in the very low ionosphere at White Sands Missile Range, New Mexico, and Wallops Island, Virginia by the parachute-borne blunt probe technique, are compared with meteorological parameters obtained from MRN Loki Darts and A3 radio wave absorption measurements. Charged particle densities are derived from the conductivities.

Between 33 and 58 Km, day-to-day variations in positive conductivity are well correlated with corresponding changes in atmospheric temperature. The temperature coefficient for positive conductivity is about an order of magnitude greater than that expected from classical theory, suggesting that positive ion mobility may be a strong function of temperature.

Day-to-day changes in the amount of relative noontime absorption reflect corresponding variations in negative conductivity at heights as low as 53 Km, indicating that coupling exists between electron densities at separate levels. This coupling most likely involves atmospheric conditions affecting electron loss rate. The results also suggest that the relative noon absorption can be predicted from early morning measurements of negative conductivity.

5.2 Suggestions for Further Research

The results discussed in this paper are somewhat tentative because of the limited amount of conductivity data available. Therefore, additional data are required before more definitive conclusions are possible. Also, current data reduction procedures must be improved so that the negative conductivity data measured above 63 Km can be utilized for analysis.

Assuming that additional conductivity data confirm the findings of this work, the physical and chemical processes occurring in the very low ionosphere would become the focus for additional research. A more sophisticated instrumentation package than the blunt probe would be required, such as one which measures not only conductivities but also ionic mobilities or charged particle densities. Also, routine measurements of temperature above 65 Km would be needed to extend certain results to higher altitudes.

In the course of this work it was observed that the relative absorption at a zenith angle of 60^{o} is well correlated, in a negative sense, with neutral density at 50 Km (see Appendix). Because this observation is independent of the blunt probe data, it is not considered in this work. However, these data are available, and they should be examined before any definitive conclusions are made.

Significant disagreements remain in the electron density profiles measured by various rocket and ground-based methods in the low ionosphere (Rowe, 1973). Because

electron density is of fundamental importance, continued progress will be difficult until a consensus can be reached on the electron density profile for this region.

REFERENCES

Ballard, H.N. and B. Rofe, in Stratospheric Circulation (Edited by W.L. Webb), Academic Press, New York, 141 (1969).

Bauer, S.J., Geofis. Para. Appl. 40, 235 (1958).

Belrose, J.S., Nature 214, 660 (1967).

Cipriano, J.P., L.C. Hale and J.D. Mitchell, paper presented at AGU meeting, San Francisco, December, 1972.

Cole, R.K. and E.T. Pierce, J. Geophys. Res. 70, 2735 (1965).

COSPAR International Reference Atmosphere, North-Holland Publishing Company, Amsterdam (1965).

Dalgarno, A., in Atomic and Molecular Processes (Edited by D.R. Bates), Academic Press, New York, 643 (1962).

Entsian, G., S.S. Gayerov and D.A. Tarasenko, Izvestiya 7, 618 (1971).

Geller, M.A. and C.F. Sechrist Jr., J. Atmosph. Terr. Phys. 33, 1027 (1971).

Gregory, J.B., J. Atmospheric Sci. 22, 18 (1965).

Hale, L.C., in Space Res. VII (Edited by R.L. Smith-Rose), North-Holland Publishing Company, Amsterdam, 140 (1967).

Hale, L.C., D.P. Hoult and D.C. Baker, Space Res. VIII (Edited by A.P. Mitra, L.G. Jacchia and W.S. Newman), North-Holland Publishing Company, Amsterdam, 320 (1968).

Heard, W.C., Sci. Report No. 297, Ionosphere Research Laboratory, Pennsylvania State University (1967).

Hoult, D.P., J. Geophys. Res. 70, 3183 (1965).

ICSU, International Council of Scientific Unions, IQSY Instruction Manual No. 4 - Ionosphere, London (1963).

Kebarle, P., S.K. Searles, A. Zolla, J. Scarborough and M. Arshadi, J. Am. Chem. Soc. 89, 6393 (1967).

Lee, M.K., Ph.D. Thesis in Electrical Engineering, The Pennsylvania State University (1973).

Loeb, L.B., Basic Processes of Gaseous Electronics, University of California Press, Berkeley (1955).

Mawdsley, J., J. Geophys. Res. 66, 1298 (1961).

McDaniel, E.S., Collision Phenomena in Ionized Gases, John Wiley and Sons, New York (1964).

Mitchell, J.D. and L.C. Hale, paper presented at COSPAR, Madrid, May, 1972, in press, Space Research XIII, North-Holland, Amsterdam.

Narcisi, R.S. and A.D. Bailey, J. Geophys. Res. 10, 3687 (1965).

Olsen, R.O., private communication (1972).

Rawer, K., ed., Winds and Turbulence in the Stratosphere, Mesosphere, and Ionosphere, Interscience, New York (1968).

Rowe, J.N., Ph.D. Thesis in Electrical Engineering, The Pennsylvania State University (1973).

Rowe, J.N., A.J. Ferraro, H.S. Lee and A.P. Mitra, J. Atmosph. Terr. Phys. 31, 1077 (1969).

Rowe, J.N. and L.C. Hale, private communication (1972).

Sechrist Jr., C.F., J. Atmosph. Terr. Phys. 29, 113 (1967).

Sechrist Jr., C.F., E.A. Mechtly, J.S. Shirke and J.S. Theon, J. Atmosph. Terr. Phys. 31, 145 (1969).

Shapley, A.H. and W.J.G. Beynon, Nature 206, 1242 (1965).

Whitten, R.C. and I.G. Poppoff, Fundamentals of Aeronomy, John Wiley and Sons, New York (1971).

APPENDIX

CORRELATION COEFFICIENTS

	σ_-	T	ρ	L_n	$L_{\chi AM}$	$L_{\chi PM}$	L_p
σ_+	1.0	.19	-.79	.60	.43	.47	.42
σ_-		.19	-.79	.60	.43	.47	.42
T			-.24	-.02	-.37	-.25	-.18
ρ	Z=30 Km			-.15	-.46	-.39	-.50
σ_+	1.0	.82	-.73	.64	.39	.41	.37
σ_-		.82	-.73	.64	.39	.41	.37
T			-.71	.49	.26	.37	.41
ρ	Z=35 Km			-.28	-.62	-.59	-.68
σ_+	.85	.91	-.62	.55	.31	.37	.32
σ_-		.78	-.56	.48	.30	.36	.34
T			-.66	.36	.24	.26	.32
ρ	Z=40 Km			-.23	-.62	.59	-.68
σ_+	.69	.82	-.46	.40	.43	.34	.42
σ_-		.36	-.51	.38	.62	.37	.54
T			-.53	-.06	.13	.12	.29
ρ	Z=45 Km			-.10	-.73	-.65	-.62
σ_+	.40	.93	-.48	.19	.50	.34	.52
σ_-		.53	-.38	.65	.47	.31	.25
T			-.42	.32	.42	.32	.45
ρ	Z=50 Km			-.37	-.85	-.81	-.87

σ_+	.33	.97	-.26	.18	.55	.35	.56
σ_-		.44	-.08	.76	.48	.38	.28
T			-.26	.29	.59	.39	.55
ρ	Z=55 Km			-.09	-.68	-.69	-.64
σ_+	.45	xx	xx	.25	.66	.46	.64
σ_-		xx	xx	.88	.52	.50	.40
L_n					.56	.69	.54
$L_{\chi AM}$						.84	.90
$L_{\chi PM}$	Z=60 Km						.92

Note: Correlation coefficients between the various L values are independent of altitude and therefore are presented only once.

Security Classification

DOCUMENT CONTROL DATA - R & D

(Security classification of title, body of abstract and indexing annotation must be entered when the overall report is classified)

1. ORIGINATING ACTIVITY (Corporate author)	2a. REPORT SECURITY CLASSIFICATION
Ionosphere Research Laboratory	2b. GROUP

3. REPORT TITLE

Relations Among Low Ionosphere Parameters and High Frequency Radio Wave Absorption

4. DESCRIPTIVE NOTES (Type of report and inclusive dates)

Scientific Report

5. AUTHOR(S) (First name, middle initial, last name)

John P. Cipriano

6. REPORT DATE	7a. TOTAL NO. OF PAGES	7b. NO. OF REFS
January 9, 1973	75	

8a. CONTRACT OR GRANT NO.	9a. ORIGINATOR'S REPORT NUMBER(S)
DA-ARO-D-31-124-72-G158 NASA NGR-39-009-218 b. PROJECT NO.	PSU-IRL-SCI-410
c.	9b. OTHER REPORT NO(S) (Any other numbers that may be assigned this report)
d.	

10. DISTRIBUTION STATEMENT

Supporting Agency

11. SUPPLEMENTARY NOTES	12. SPONSORING MILITARY ACTIVITY
	U. S. Army Research Office - Durham National Aeronautics and Space Administration

13. ABSTRACT

Charged particle conductivities measured in the very low ionosphere at White Sands Missile Range, New Mexico, and Wallops Island, Virginia, are compared with atmospheric parameters and high frequency radio wave absorption measurements. Charged particle densities are derived from the conductivity data. Between 33 and 58 km, positive conductivity correlated well with neutral atmospheric temperature, with temperature coefficient as large as $4.6\%^{o}K^{-1}$. Good correlations were also found between HF radio wave absorption and negative conductivity at altitudes as low as 53 km, indicating that the day-to-day absorption variations were principally due to variations in electron loss rate.

DD FORM 1 NOV 65 1473 (PAGE 1)

S/N 0101-807-6811

NONE

Security Classification

A-31408